JCI The Journal of Clinical Investigation

The cardiomyocyte disrupts pyrimidine biosynthesis in non-myocytes to regulate heart repair

Shen Li, … , Caius G. Radu, Arjun Deb

J Clin Invest. 2021. https://doi.org/10.1172/JCI149711.

Research In-Press Preview Cardiology

Graphical abstract

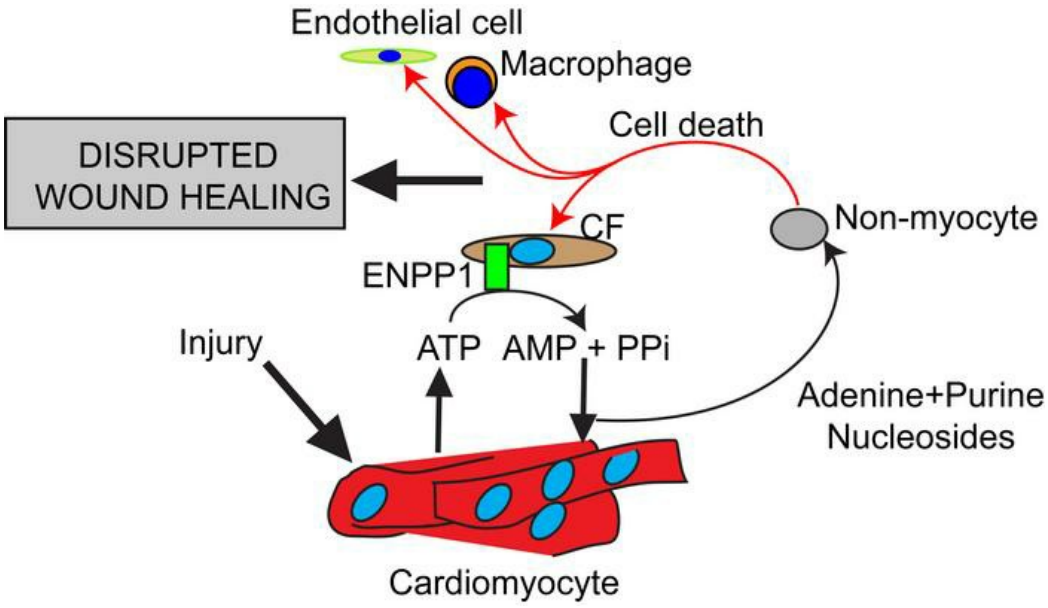

The cardiomyocyte disrupts pyrimidine biosynthesis in non-myocytes to regulate heart repair

Shen Li[1,2,3,4,5,6], Tomohiro Yokota[1,2,3,4,5,6], Ping Wang[1,2,3,4,5,6], Johanna ten Hoeve[7], Feiyang Ma[3,4,5], Thuc M. Le[7,13,17], Evan R. Abt[7,13,17], Yonggang Zhou[1,2,3,4,5,6], Rimao Wu[1,2,3,4,5,6], Maxine Nathavongdouangsy[1,2,3,4,5,6], Abraham Rodriguez[1,2,3,4,5,6], Yijie Wang[1,2,3,4,5,6], Yen-Ju Lin[6,14,20], Hayato Muranaka[16,17], Mark Sharpley[3,4,5], Demetrios T. Braddock[8], Vicky E MacRae[9], Utpal Banerjee[3,4,5,10], Pei-Yu Chiou[6,14,20], Marcus Seldin[11], Dian Huang[4,6,12,13], Michael Teitell[4,6,12,13], Ilya Gertsman[19], Michael Jung[15], Steven J Bensinger[16,17], Robert Damoiseaux[6,13,14,17], Kym Faull[18], Matteo Pellegrini[3,4,5], Aldons J Lusis[1,2,16], Thomas Graeber[7,13,17], Caius G Radu[7,13,17] & Arjun Deb*[1,2,3,4,5,6].

[1]Division of Cardiology, Department of Medicine, David Geffen School of Medicine, University of California, Los Angeles, CA 90095, U.S.A.
[2]UCLA Cardiovascular Theme, David Geffen School of Medicine, University of California, Los Angeles
[3]Department of Molecular, Cell and Developmental Biology, College of Life Sciences, University of California, Los Angeles, CA 90095, U.S.A.
[4]Eli & Edythe Broad Center of Regenerative Medicine and Stem Cell Research, University of California, Los Angeles, CA 90095, U.S.A.
[5]Molecular Biology Institute, University of California, Los Angeles, CA 90095
[6]California Nanosystems Institute, University of California, Los Angeles, CA 90095.
[7]UCLA Metabolomics Center, Crump Institute of Molecular Imaging, California Nanosystems Institute, University of California, Los Angeles, CA 90095, U.S.A
[8]Department of Pathology, Yale University, New Haven, CT 06520, U.S.A.
[9]Division of Functional Genetics and Development, The Roslin Institute and R(D)VS, University of Edinburgh, U.K.
[10]Department of Biological Chemistry, David Geffen School of Medicine, University of California, Los Angeles, CA 90095, U.S.A.
[11]Department of Biological Chemistry and Center for Epigenetics and Metabolism, University of California, Irvine, CA 92697.
[12]Department of Pathology, David Geffen School of Medicine, University of California, CA 90095, U.S.A.
[13]Jonsson Comprehensive Cancer Center, David Geffen School of Medicine, University of California, CA 90095, U.S.A.
[14]Department of Bioengineering, Samueli School of Engineering at UCLA, Los Angeles, CA 90095, USA
[15]Department of Chemistry, College of Physical Sciences, University of California, Los Angeles, CA 90095, U.S.A.
[16]Department of Microbiology, Immunology and Molecular Genetics, University of California, Los Angeles, CA 90095, U.S.A.
[17]Department of Molecular and Medical Pharmacology, David Geffen School of Medicine, University of California, Los Angeles, CA 90095
[18]Pasarow Mass Spectrometry Laboratory, Jane and Terry Semel Institute for Neuroscience and Human Behavior and Department of Psychiatry & Biobehavioral Sciences, David Geffen School of Medicine at UCLA, Los Angeles, CA 90095, USA
[19]Clarus Analytical, San Diego, CA 92126
[20] Department of Mechanical and Aerospace Engineering, University of California, Los Angeles, CA 90095, USA

*Correspondence
Arjun Deb, M.D.
McDonald Research Laboratories 3609A,
675 Charles E Young Drive S,
University of California, Los Angeles, CA 90095
Email: adeb@mednet.ucla.edu
Phone: 310-983-1017

Conflict of interest: Intellectual property related to this body of work (Patent No: 17/306,544 and 62/421739) has been filed and assigned to the Regents of the University of California. Arjun Deb and Michael Jung are co-founders and hold equity in Westwood Therapeutics, aimed at therapeutics related to ENPP1 inhibition.

Abstract
Various population of cells are recruited to the heart after cardiac injury but little is known about whether the cardiomyocyte directly regulates heart repair. In a murine model of ischemic cardiac injury, we demonstrate that the cardiomyocyte plays a pivotal role in heart repair by regulating nucleotide metabolism and fates of non-myocytes. Cardiac injury induced the expression of the ectonucleotidase ENPP1 that hydrolyzes extracellular ATP to form AMP. In response to AMP, the cardiomyocyte released adenine and specific ribonucleosides that disrupted pyrimidine biosynthesis at OMP synthesis step, induced genotoxic stress and a p53 mediated cell death of cycling non-myocytes. As non-myocytes are critical for heart repair, we showed that rescue of pyrimidine biosynthesis by administration of uridine or by genetic targeting of ENPP1/AMP pathway enhanced repair after cardiac injury. We identified ENPP1 inhibitors on small molecule screening and showed that systemic administration of an ENPP1 inhibitor after heart injury rescued pyrimidine biosynthesis in non-myocyte cells, augmented cardiac repair and post infarct heart function. These observations demonstrate that the cardiac muscle cell by releasing adenine and specific nucleosides after heart injury regulates pyrimidine metabolism in non-muscle cells and provide insight into how inter-cellular regulation of pyrimidine biosynthesis can be targeted and monitored for augmenting tissue repair.

Keywords: Adenine, ENPP1, pyrimidine biosynthesis, cardiac repair, nucleosides

Introduction

Myocardial infarction (MI) is a leading cause of systolic heart failure(1). After MI, different cell types are recruited to the heart in a spatio-temporally regulated manner to contribute to wound healing. An initial polymorphonuclear infiltrate is replaced by macrophages and vital cues provided by inflammatory cells initiate fibroblast and endothelial cell proliferation to form granulation tissue (2, 3) that subsequently matures to form a scar (4). The presence of different types of cells within the injured heart enables cell-cell crosstalk and regulation of different phases of wound healing(3, 5). Although the cellular events in cardiac repair have been well studied, the role of the cardiac muscle cell itself in regulating cardiac wound healing is unclear. The cardiac muscle cell does not possess any ontogenetic memory of acute injury and whether it can directly regulate organ repair remains an unanswered question.

In this report, we demonstrate that the cardiac muscle cell plays a pivotal role in regulating the cardiac repair response by releasing metabolites that disrupt cellular function of non-myocyte cells such as macrophages, fibroblasts, endothelial and smooth muscle cells and worsens wound healing. Following ischemic cardiac injury, the extracellular ATP levels increase in the injured region from extravasation of intracellular ATP from necrotic myocytes, increased membrane permeability and upregulated activity of nucleotide transporters(6-8). ATP is a damage associated molecular pattern (DAMP) signal associated with acute injury(9). Increased accumulation of extracellular ATP is limited by tissue ectonucleotidases, which are membrane bound enzymes with an extracellular catalytic domain that hydrolyzes extracellular ATP. We show that the ectonucleotidase, ENPP1, (10) is induced after cardiac injury and is the principal

nucleotidase that hydrolyzes extracellular ATP in the injured heart. AMP generated from ENPP1 activity induces the cardiomyocyte to release adenine base and specific purine nucleosides, that in combination disrupts pyrimidine biosynthesis in non-myocytes. Pyrimidine biosynthetic defects adversely alter purine/pyrimidine ratios in non-myocytes during cell proliferation and induce a DNA damage response that leads to cell death of non-myocytes. Macrophages, endothelial cells and fibroblasts are critical components of cardiac repair and depletion or functional impairment of non-myocyte cells is known to worsen cardiac wound healing(11). We demonstrate that genetic or pharmacologic targeting of the ENPP1/AMP cascade in the injured heart attenuates cardiomyocyte induced defects of pyrimidine biosynthesis in non-myocytes and leads to superior post infarct cardiac function. Taken together, these observations shed insight into the role of the cardiac muscle cell in regulating nucleotide metabolism and cellular function of non-myocytes and how such myocyte induced defects of pyrimidine biosynthesis in cycling non-myocytes can be specifically targeted to enhance repair and post injury heart function.

Results

Cardiac injury induces expression of ENPP1, which is the principal ectonucleotidase that hydrolyzes extracellular ATP

We subjected adult mice to ischemic cardiac injury by permanent ligation of the left anterior descending coronary artery and performed qPCR on injured and uninjured regions of hearts at 3,7,14 and 21 days post injury. ENPP1 expression increased by 5-fold on Day 3 and was 15-20 fold higher at Day 7 compared to uninjured regions **(Fig 1A)**. Western Blotting confirmed increased ENPP1 protein expression **(Fig 1B)**. We

next measured ENPP1 enzymatic activity and observed that ATP hydrolytic activity was significantly increased in the injured tissue homogenates, suggesting that increased ENPP1 protein was associated with increased ectonucleotidase activity (**Fig 1C**). As there are several members of the ectonucleotidase family(12, 13) that hydrolyze extracellular ATP, we analyzed RNA-seq data sets of acute cardiac injury(14) and observed that of the known mammalian ectonucleotidases, ENPP1 was the only one that demonstrated the most early, robust and consistent increase in expression (**Fig 1D**). To confirm that increased ectonucleotidase acgivity in injured cardiac tissue is predominantly due to increased ENPP1, we subjected ENPP1 mutant mice ($ENPP1^{asj/asj}$ mice) to ischemic cardiac injury. The $ENPP1^{asj/asj}$ mice have an amino acid substitution in the catalytic domain that renders the catalytic domain devoid of ATP hydrolytic activity(15). In contrast to wild type mice, injured heart tissue from $ENPP1^{asj/asj}$ animals did not show increased ATP hydrolytic activity (**Fig 1E**). Taken together these observations demonstrate that following cardiac injury, ENPP1 expression and activity increase significantly and ENPP1 is the principal nucleotidase that hydrolyzes extracellular ATP.

Immunostaining demonstrated robust increase in ENPP1 expression that was predominantly restricted to the injury region **(Fig 1F,G**). To identify the phenotype of the cell expressing ENPP1, we isolated myocytes and non-myocytes from the injured heart and observed that ENPP1 expression was restricted to the non-myocyte fraction of cells (**Fig S1A**). Expression of ENPP1 was almost 100-fold higher in non-myocytes (**Fig S1B**) and immunostaining demonstrated that ENPP1 expressing cells resided in the myocardial interstitium and (**Fig S1C**) and co-stained for the cardiac fibroblast marker

vimentin (**Fig 1H**). To confirm this observation, we performed immunostaining in mice harboring genetically labeled cardiac fibroblasts. We crossed Col1a2CreERT2 (16) mice or TCF21MerCreMer(MCM) (17) (TCF21 and Col1a2 being fibroblast Cre drivers) mice with the lineage reporter Rosa26tdTomato mice. Mice were administered tamoxifen to label fibroblasts and and immunostaining of injured heart sections demonstrated ENPP1 to be expressed by genetically labeled cardiac fibroblasts (**Fig 1I,J**). Flow cytometry on the injured heart demonstrated a two fold increase in the number of ENPP1 expressing cells (**Fig S1D**) and 68%,72% and 86% of ENPP1 expressing cells co-expressed the fibroblast markers CD90.2, TCF21MCM induced tdTomato label and MEFSK4 respectively (**Fig S1D**). Macrophages and endothelial cells comprised the remaining fraction of non-myocyte cells expressing ENPP1 (**Fig S1E,F**). We also analyzed single cell RNA-seq data sets of the non-myocyte fraction(14) isolated at 7 days after ischemic cardiac injury and consistent with flow cytometry and immunostaining, observed that ENPP1 was primarily expressed by cardiac fibroblasts and to a lesser degree by macrophages and endothelial cells (**Fig 1K**).

Increased ENPP1 expression in non-myocytes induces the cardiomyocyte to secrete pro-apoptotic molecules that cause cell death of non-myocytes

Extracellular ATP is a damage associated molecular pattern (DAMP) signal and is known to increase by several orders of magnitude after tissue injury(18). We hypothesized that ENPP1 via its ATP hydrolytic activity regulates intercellular communication between myocytes and non-myocytes in the injured region. We first over-expressed the mouse ENPP1 gene in cardiac fibroblasts (CFs) using a lentivirus and immortalized ENPP1 over-expressing cardiac fibroblasts with the SV40 antigen

(ENPP1-CFs) to avoid culture induced senescence and variation associated with primary cell isolation (**Fig S2A,B**). Control cardiac fibroblasts (Control-CFs) infected with an empty lentivirus were also immortalized in a similar manner. To determine the role of ENPP1 in mediating myocyte-non myocyte cross talk, we co-cultured ENPP1-CFs and Control CFs with neonatal rat ventricular cardiomyocytes (NRVM) and then added ATP. Within 48 hours of incubation, we observed there was a 75% reduction in the number of ENPP1-CFs with no effect on the numbers of cardiomyocytes (**Fig 2A,B**)**.** In the absence of ATP, there was no reduction in ENPP1-CFs, and ATP did not significantly affect the cell numbers of Control-CFs co-cultured with cardiomyocytes (**Fig 2B**). In the absence of co-culture with cardiomyocytes, addition of ATP did not result in reduction of ENPP1-CFs (**Fig 2C**). These observations strongly suggest that an interaction between ENPP1-CFs, ATP and cardiomyocytes was causing cell death of cardiac fibroblasts.

Considering these observations, we hypothesized that the combination of ENPP1 and ATP was inducing the cardiomyocytes to secrete molecules that were causing death of CFs. To investigate this hypothesis, we added ATP and recombinant ENPP1 protein to NRVM. Following 24 hours of incubation, we collected the conditioned medium and then treated CFs (grown in a separate plate in the absence of any cardiomyocytes) with the myocyte conditioned medium (MCndM) so collected (**Fig 2D**). Control myocyte conditioned medium included conditioned medium collected from NRVM in an identical manner after treatment with either vehicle, ENPP1 or ATP respectively. Within 48 hours of addition of ENPP1+ATP MCndM, CFs underwent cell death (**Fig 2D**). Propidium iodide (PI) and Annexin V staining with flow cytometry

confirmed a significant increase in cell death of CFs treated with ENPP1+ATP MCndM compared to control MCndM. (**Fig 2E**). TUNEL staining and cleaved caspase 3 activity confirmed the apoptotic cell death of CFs. (**Fig 2F,G**). To make sure that the immortalization process itself did not make the CFs sensitive to MCndM, we isolated primary CFs, treated them with ENPP1+ATP MCndM and observed a similar degree of cell death (**Fig S2C,D**). These observations strongly suggest that in response to ENPP1 protein and ATP, the cardiomyocytes secrete pro-apoptotic molecules that induce cell death of CFs but not of myocytes themselves.

To determine whether the ability to secrete pro-apoptotic molecules was a specific property of cardiomyocytes, we added ENPP1 recombinant protein and ATP to CFs. Transfer of ENPP1+ATP CF conditioned medium to CFs grown separately in another plate did not cause cell death (**Fig S2E**). These observations thus show that the ability to secrete pro-apoptotic small molecules in the presence of ENPP1 and ATP is specific to cardiomyocytes. Next, we investigated whether human cardiomyocytes exhibited this property of secreting pro-apoptotic molecules. We induced cardiomyogenic differentiation of human pluripotent stem cells (hPSCs), treated hPSC derived cardiomyocytes with ENPP1 and ATP (**Fig S2F**), collected the conditioned medium, added it to human cardiac fibroblasts grown in a separate dish and observed a similar degree of cell death (**Fig S2G,H**). These observations confirm the ability of human cardiomyocytes to respond to ENPP1 and ATP in a similar manner as rodent cardiomyocytes.

We next investigated whether the ectonucleotidase activity of ENPP1 was required for this interaction with cardiomyocytes to generate pro-apoptotic molecules.

We created an expression construct for a mutant ENPP1 (mutant ENPP1, containing a single amino acid substitution in the catalytic domain)(15), that is devoid of nucleotidase activity (**Fig S2I**). We lentivirally overexpressed the mutant ENPP1 construct in CFs and subsequently immortalized them (mutant ENPP1-CFs). When mutant ENPP1-CFs or control ENPP1-CFs were co-cultured with NRVM, the addition of ATP induced cell death of ENPP1-CFs whereas minimal cell death was observed in mutant ENPP1-CFs (**Fig S2J,K**). These experiments thus demonstrate that the catalytic domain of ENPP1 is necessary for the cardiomyocytes to generate pro-apoptotic molecules. ENPP1 hydrolyzes extracellular ATP directly into adenosine monophosphate (AMP) and pyrophosphate (PPi), and so if the catalytic domain of ENPP1 is necessary for the myocytes to generate pro-apoptotic molecules, it follows that either AMP or PPi alone should be able to induce the cardiomyocyte to secrete proapoptotic molecules. We added AMP or PPi to cardiomyocytes, collected the MCndM after 24 hours and then added the MCndM to CFs grown separately. AMP MCndM caused cell death but not PPi MCndM (**Fig 2H,I**). However, the addition of AMP alone to CFs did not induce cell death thus excluding a potential toxic effect of AMP alone on CFs (**Fig S2L**). These observations thus demonstrate that AMP, a product generated by ENPP1 mediated hydrolysis of ATP, induces the myocyte to generate pro-apoptotic molecules that cause cell death of CFs.

We next investigated the dynamics of cell death and performed quantitative phase microscopy (QPM) to determine the biomass of numerous individual CFs following treatment with MCndM. As cells undergo apoptosis, the surface area and the cell biomass of the affected cells decreases (19). We observed that CFs treated with

ENPP1+ATP MCndM exhibited an increasing cell biomass with stable cell surface area for the first 12 hours, similar to CFs treated with control MCndM medium (**Fig S2M,N**). After 12 hours, CFs treated with ENPP1+ATP MCndM exhibited a rapid and significant decline in cell biomass and cell surface area due to apoptosis (**Fig S2M,N, Movie S1**). Plots of single cell surface area versus individual biomass clearly demonstrated significant mean differences in cell size and biomass of CFs after 24 hours of treatment with ENPP1+ATP MCndM versus control MCndM (**Fig S2O,P**).

In addition to CFs, macrophages and endothelial cells also expressed ENPP1 after cardiac injury. We added ENPP1+ATP MCndM to macrophages, endothelial or smooth muscle cells grown separately and observed that conditioned medium was able to induce cell death in these non-myocyte population as well (**Fig 2J,K**). However, ENPP1 and ATP MCndM did not induce cell death of cardiomyocytes grown separately (**Fig 2L**) and neither did it affect myocyte contractility (**Fig S3A,B**). These observations demonstrate that in response to ENPP1+ATP, cardiomyocyte secreted pro-apoptotic molecules can cause cell death of a wide variety of non-myocyte cells but the myocyte itself remains immune to such death inducing molecules.

Genetic deletion of ENPP1 leads to enhanced cardiac wound healing

Before determining the identity of the pro-apoptotic molecules secreted by myocytes, we investigated the physiological role of ENPP1 in regulating cardiac wound healing in vivo. Cardiac fibroblasts, macrophages, endothelial cells and smooth muscle cells play a vital role in cardiac repair after ischemic cardiac injury. We hypothesized that if increased ENPP1 expression in the heart promotes the cardiac muscle cell to secrete molecules that exert adverse effects on non-myocyte cells, then cardiac repair should

be augmented by inhibiting ENPP1. Better preservation of post injury cardiac function, increased angiogenesis, decreased inflammation and decreased post injury scar size were defined by us as quantifiable metrics to characterize cardiac wound healing.

As ENPP1 expression significantly overlapped with the expression of Col1a2 in on single cell RNA-seq (**Fig S1G**), we used the Col1a2CreERT driver to conditionally delete ENPP1 in cardiac fibroblasts. We crossed the Col1a2CreERT animals with animals that had both ENPP1 alleles floxed ($ENPP1^{fl/fl}$) (20) and progeny mice were administered tamoxifen from 5 days prior to cardiac injury to 7 days after to maximize ENPP1 deletion (ENPP1 conditional knockout or ENPP1CKO). Western blotting confirmed decreased ENPP1 expression in the injured area (**Fig 3A,B**). On serial echocardiography, ENPP1CKO animals demonstrated significantly better cardiac function and decreased chamber size within 7 days of injury compared to control littermates (**Fig 3C,D**). We defined mild, moderate or severe depression in post injury cardiac contractile function as EF>40%, between 20% and 40% and less than 20% respectively. Only 6% of the animals in the ENPP1CKO group exhibited severe depression in EF compared to almost 50% in control littermates (**Fig 3E, Table S1A**). The degree of fibrosis or scar size measured at 4 weeks post injury was significantly lower in the ENPP1CKO animals (**Fig 3F,G**). We again classified the scar size as mild (<20%), moderate (20-40%) and severe (>40% of LV surface area) and observed that approximately 21% of the control animals exhibited severe fibrosis at 4 weeks after MI in contrast to less than 6.2% in the ENPP1CKO animals (**Fig 3H, Table S1B**). Post infarct hypertrophy is an adverse outcome of wound healing (21) and we observed that the heart weight/body weight ratio was significantly lower in the ENPP1CKO animals

(**Fig 3I**). Histology of the peri-infarct area confirmed significantly decreased myocyte surface area in ENPP1CKO hearts (**Fig 3J**). Capillary density was significantly increased in the ENPP1CKO animals at 4 weeks after injury (**Fig 3K**). These observations demonstrate that cardiac wound healing is significantly enhanced in ENPP1CKO animals with better preservation of post injury function, greater angiogenesis, significantly decreased scarring and post injury cardiac hypertrophy.

Genetic variation of ENPP1 in heart predicts adverse cardiac outcomes across 100 diverse strains of mice

To further strengthen our observations on the role of ENPP1 in regulating cardiac wound healing, we employed a systems genetics approach using alternative models of cardiac injury. The hybrid mouse diversity panel comprises 100 diverse classical and recombinant inbred strains of mice which can be subjected to cardiac injury to identify genetic determinants of post injury cardiac traits (22, 23). The mouse strains in the HMDP were treated with 3 weeks of continuous isoproterenol infusion that results in cardiomyocyte hypertrophy and interstitial fibrosis. Animals were followed by serial echocardiograms to determine ejection fraction and hearts harvested to determine LV gene expression changes. Gene expression signatures were statistically correlated with clinical traits to identify significant relationships across all the strains. Using this system, we initially observed a large degree of genetic variation in ENPP1 expression, particularly following isoproterenol infusion (**Fig 4A**). Next, we analyzed the association of genes versus traits and observed that ENPP1 expression significantly correlated with the development of adverse post injury traits such as LV hypertrophy (cardiac mass), chamber size, decreased cardiac contractility and degree of fibrosis following

isoproterenol infusion **(Fig 4B-F)**. As a control, we examined a cardiac phenotype unrelated to wound healing such as heart rate and did not see any significant correlation with ENPP1 expression (**Fig 4G**). These observations using systems genetics approaches provide compelling evidence that ENPP1 is a strong driver of cardiac repair.

Single cell RNA-seq of injured ENPP1CKO hearts demonstrates downregulation of pro-inflammatory, apoptotic and fibrotic pathways

To investigate mechanisms of enhanced cardiac repair in ENPP1CKO animals, we performed single cell RNA-seq of non-myocytes in control and ENPP1CKO hearts at 7 days following injury to determine changes in cell specific transcriptional signatures. We observed fibroblasts, macrophages and endothelial cells as the largest contributors to the non-myocyte population (**Fig S4A, 5A**). Increased numbers of endothelial cells and fibroblasts were observed in ENPP1CKO hearts consistent with the pro-apoptotic effect of ENPP1/AMP mediated metabolic cascade (**Fig 5B,C**). Macrophages were decreased likely reflecting decreased non-myocyte cell death and attenuation of the inflammatory response (**Fig 5B,C**). Next, we specifically examined the cardiac fibroblast population and first confirmed decreased ENPP1 expression (**Fig 5D**). Myofibroblasts are activated fibroblasts that secrete matrix proteins to form scar tissue and the number of myofibroblasts, identified by α smooth muscle actin expression (αSMA) was decreased in ENPP1CKO hearts (**Fig 5E,F**). Other markers of activated myofibroblasts such as Cnn2 (calponin) and Tagln (transgelin)(14) were also decreased (**Fig 5G**). Immunostaining for αSMA confirmed the decrease in myofibroblasts (**Fig 5H,I**).

Gene ontology demonstrated downregulation of extracellular matrix (ECM) organization, inflammatory and apoptotic pathways in cardiac fibroblasts (**Fig 6A**). Canonical genes known to regulate ECM deposition were significantly downregulated in cardiac fibroblasts in ENPP1CKO animals (**Fig 6B**). Analysis of apoptotic pathways demonstrated downregulation of pro-apoptotic genes or genes inducing growth arrest and upregulation of anti-apoptotic genes in CFs of ENPP1CKO animals (**Fig 6C**). The average expression of pro-apoptotic genes (apoptosis module score) was significantly lower in ENPP1CKO CFs (**Fig S4B**) and immunostaining confirmed decreased numbers of apoptotic CFs in ENPP1CKO animals at 3,7 and 14 days after cardiac injury (**FigS4C,D**). The average expression of cell cycling genes (cell cycle module score) in CFs of ENPP1CKO hearts was higher compared to that in control littermates (**Fig S4E**) and immunostaining confirmed a higher fraction of proliferating CFs in the ENPP1CKO hearts (**Fig S4F,G**). Taken together these observations suggest that even though fibroblast numbers are increased with decreased apoptosis of cardiac fibroblasts in the ENPP1CKO hearts, myofibroblast activation and expression of canonical ECM genes is significantly decreased. Macrophages in ENPP1CKO hearts also exhibited decreased expression of pro-inflammatory genes (**Fig 6D**). Histology at 7 days post injury showed decreased collagen deposition (**Fig 6E,F**) along with a significantly decreased number of macrophages and increased number of capillaries (**Fig 6G,H**), findings consistent with the RNA-seq analysis. Immunostaining confirmed significantly decreased number of apoptotic endothelial cells in the hearts of ENPP1CKO animals (**Fig S4H,I**) associated with a higher cell cycle module score (**Fig S4J**) suggesting that a greater number of endothelial cells in the ENPP1CKO hearts are likely secondary to both

increased survival and proliferation. Examination of surviving myocardium with TTC staining at 24 hours following injury however did not demonstrate any differences between the ENPP1CKO and control hearts (**Fig S4K,L**). Immunostaining confirmed no significant differences in the number of apoptotic myocytes between the control and ENPP1CKO animals (**Fig S4M,N**), thereby suggesting the beneficial effects on cardiac function are likely secondary to augmented cardiac repair and attenuation of adverse post infarct remodeling rather than due to a greater amount of surviving myocardium.

Fibrosis after cardiac injury is a complex phenotype regulated by multiple factors such as the degree of inflammation, the amount of neovascularization or post infarct angiogenesis, myofibroblast activation and mechanical properties of the ECM that provide feedback for ECM deposition(14). Even though fibroblast apoptosis was decreased and led to a higher number of cycling fibroblasts in the ENPP1CKO hearts, the degree of myofibroblast activation and overall ECM gene expression was significantly attenuated. ENPP1CKO animals exhibited lesser degrees of endothelial cell apoptosis and greater post infarct angiogenesis. Decreased inflammation and decreased non-myocyte cell death could have contributed to decreased activation of fibroblasts and superior cardiac remodeling in ENPP1CKO hearts. Thus, augmented non-myocyte survival leads to superior tissue repair independent of initial myocyte cell death. Genetic deletion of ENPP1 switches the wound healing transcriptional response after cardiac injury to a more pro-reparative one with less inflammation, less scarring and greater angiogenesis.

Cardiomyocyte secreted metabolites rather than proteins cause cell death of non-myocytes.

We next sought to identify the pro-apoptotic molecules secreted by cardiomyocytes in response to the presence of ATP and ENPP1. We first determined whether the pro-apoptotic molecules were proteins or metabolites. We collected the ENPP1+ATP MCndM and subjected it to high heat (95°C) for 15 minutes to enable denaturation of proteins (**Fig S5A**). When added to cardiac fibroblasts, the heat-treated MCndM retained biological activity and induced CF cell death (**Fig S5B**). To confirm these results, we next passed the ENPP1+ATP MCndM through a protein fractionation column with a filter cutoff of 3 kilo Daltons (kD) (**Fig S5C**) and then treated CFs with the protein rich (>3kD) or protein poor fractions (<3kD) of the MCndM. The protein rich fraction (MW>3kD) did not cause cell death but the MCndM filtrate less than 3kD induced cardiac fibroblast cell death (**Fig S5D**). These observations taken together suggest that metabolites rather than proteins secreted by cardiomyocytes are causing cell death of non-myocyte cells.

To determine the identity of the metabolites, we collected MCndM following treatment of the myocytes with ENPP1, ATP, ENPP1+ATP, AMP or PPi and subjected the conditioned medium to LC-MS analysis. We identified metabolites that were differentially present between ENPP1+ATP or AMP treated MCndM versus control MCndM. These metabolites mainly related to purine/pyrimidine biosynthesis/catabolism pathways and did not include any known pro-apoptotic factors (**Fig S5E,F**). We treated CFs with each of the top 7 most differentially upregulated metabolites in the

ENPP1+ATP or AMP MCndM but none of these metabolites caused cell death (**Fig S5F,G**).

Death of non-myocytes is related to cell proliferation

Unable to readily identity the pro-apoptotic metabolites, we sought alternative physiologic principles of approaching the problem. We hypothesized that the ability of myocytes to be immune to the conditioned medium likely reflects an inherent cellular property of myocytes that distinguishes itself from that in non-myocyte cells. As non-myocytes are proliferative and myocytes are non-proliferative, we hypothesized that the ability to cycle was making the non-myocytes susceptible to the metabolites secreted by the myocyte. To determine whether this was true, we irradiated cardiac fibroblasts and observed that the ENPP1+ATP MCndM could not induce death of irradiated CFs in contrast to non-radiated control CFs (**Fig 7A,B**). To confirm this finding, we next treated CFs with the cell cycle inhibitor mitomycin C and again observed cell cycle arrested CFs were resistant to ENPP1+ATP MCndM induced cell death (**Fig 7C,D**). To obtain an independent confirmation on the cell cycle dependent cell death of cardiac fibroblasts treated with ENPP1+ATP myocyte conditioned medium, we repeated the experiments with primary mouse embryonic fibroblasts (mEF) and confirmed that cell cycle arrest with irradiation or mitomycin C prevented cell death of mEF (**Fig 7E-H**). These observations suggest that cell cycling of the target non-myocyte cells is necessary for the myocyte secreted molecules to cause cell death.

We next examined the mechanisms of cell death secondary to cell cycling. We performed RNA-seq on CFs treated ENPP1+ATP MCndM. Principal component analysis demonstrated that the gene expression signatures of CFs treated with

ENPP1+ATP or AMP MCndM were similar and clearly distinguishable from those of the other groups (**Fig 7I**). Gene ontogeny analysis demonstrated significant upregulation of the p53 signaling pathway (**Fig 7J**) with significant differential expression of p53 regulated pro-apoptotic genes (**Fig 7K**) including canonical apoptotic modulators such as Bax, Bak and BCl2 (**Fig 7K**). Myocytes remained immune to ENPP1+ATP MCndM and did not exhibit changes in p53 driven apoptosis genes (**Fig S3C**). As cell death was related to cycling, we next examined in detail the phases of cell cycle that were disrupted in non-myocytes treated with ENPP1+ATP MCndM. CFs demonstrated evidence of G1/S phase arrest (**Fig 7L,M**). Western blotting demonstrated significant upregulation of DNA damage response markers (Gamma H2A.X) and the checkpoint kinase 1 (pCHK1) that is known to regulate a DNA damage response and cell cycle arrest (**Fig 7N**). Phosphorylation of serine15 in p53 has been shown to initiate DNA damage response(24, 25) and we observed increased phosphorylation of p53Ser15 in CFs treated with ENPP1+ATP MCndM **(Fig 7O)**. To determine whether a p53 initiated DNA damage response was required for cell death, we deleted the p53 gene in cardiac fibroblasts by infecting primary CFs isolated from p53 floxed mice(26) with a lentiviral Cre (**Fig 7P**). CFs deficient in p53 were resistant to ENPP1+ATP MCndM induced cell death (**Fig 7Q,R).** These experiments thus demonstrate that metabolite/s secreted by the cardiac muscle cell in response to ENPP1 and ATP initiate a p53 dependent DNA damage response and apoptosis in cycling non-myocyte cells.

Myocyte secreted metabolite(s) disrupt pyrimidine biosynthesis in cycling non-myocytes to cause cell death

The experiments related to the ability of ENPP1+ATP MCndM to initiate a DNA damage

response in cycling non-myocyte cells strongly suggested that the metabolite(s) interfere with the cell cycle machinery. A nucleotide balance between the content of purines and pyrimidines available to cycling cells is critical to avoid genotoxic stress and maintain genomic stability (27). We hypothesized that disruption of the nucleotide biosynthetic pathways in non-myocyte cells and an imbalance of purine versus pyrimidine nucleotides was inducing genotoxic stress and initiating a DNA damage response in proliferating non-myocytes. We treated CFs with ENPP1+ATP MCndM for 24 hours and measured the content of nucleoside monophosphate and triphosphates by LC/MS-MS. Consistent with our hypothesis, we observed that the pyrimidines cytidine and uridine mono and triphosphates (CMP, CTP, UMP, UTP) were significantly reduced in ENPP1+ATP MCndM treated CFs (**Fig 8A**) while purine nucleotide levels were slightly increased or remained unaltered (**Fig 8B**). These observations suggested that insufficient pyrimidine precursors during cell cycling were likely leading to a DNA damage response. We next attempted to rescue cell death of CFs by adding uridine or deoxycytidine to CFs treated with ENPP1+ATP MCndM (**Fig 8C**) and observed that addition of uridine or deoxycytidine or both completely rescued cell death **(Fig 8D,E)**. Deoxycytidine serves as a precursor of dCTP synthesis via the enzyme deoxycytidine kinase. When we added a specific inhibitor of deoxycytidine kinase (DI-87), deoxycytidine was unable to prevent cell death thereby strongly supporting the hypothesis that pyrimidine deficiency was causing cell death (**Fig 8F,G**).

Inhibition of UMP synthase step is the underlying cause of defects in pyrimidine biosynthesis

Pyrimidine biosynthesis occurs via a sequence of well-regulated steps where

dihydroorotate formed from carbamoyl phosphate gives rise to orotate and subsequently the important intermediate OMP. (**Fig 8H)**. To determine which steps in pyrimidine biosynthesis are affected in cycling non-myocytes, we treated CFs with ENPP1+ATP MCndM for 24 hours and subjected the CFs to mass spectrometry to determine metabolites in the pyrimidine biosynthesis pathway. CFs treated with ENPP1+ATP MCndM showed significantly increased amounts of carbamoyl aspartate, dihydroorotate and orotate but decreased orotidine, uridine, UMP, UDP, UTP as well as CTP **(Fig 8I)**. This suggests that the ENPP1+ATP MCndM is inhibiting later steps of uridine monophosphate (UMP) synthesis in CFs. As orotate levels were increased but orotidine levels decreased in ENPP1+ATP MCndM treated CFs, we hypothesized that inhibition was occurring at the OMP synthesis step from orotate and PRPP. OMP added to CFs completely rescued cell death **(Fig 8J,K)** thereby strongly suggesting that the ENPP1+ATP MCndM inhibits pyrimidine biosynthesis at the OMP synthesis step in cycling non-myocytes. Finally, to demonstrate that defects in pyrimidine biosynthesis are sufficient to cause cell death, we treated CFs with a specific inhibitor of DHODH (brequinar) and observed cell death thereby demonstrating that disruption in pyrimidine biosynthesis is sufficient to cause cell death (**Fig 8L,M**).

Adenine is a critical pro-apoptotic metabolite secreted by cardiomyocytes.

We returned to the central question of the identity of cardiomyocyte derived pro-apoptotic metabolites. As the metabolites were inhibiting pyrimidine biosynthesis, we hypothesized that the metabolites were likely nucleotides or their derivatives. We performed high performance liquid chromatography (HPLC) to determine physico-chemical properties of the candidates. We joined two reverse phase HPLC columns in

series, loaded ENPP1+ATP MCndM onto the columns and used a linear gradient of acetonitrile (ACN) to collect 80 fractions (**Fig S6A**). Pools of 10 fractions were vacuum dried, reconstituted, and added to CFs and we observed that fractions 41-50 from ENPP1+ATP MCndM (corresponding to ACN concentrations of 40-50%) reliably resulted in CF cell death, while those of control MCndM did not (**Fig S6B,C**). To confirm these observations, we loaded a C18 stationary phase column with ENPP1+ATP MCndM, eluted fractions in a similar manner and observed cell death only with the 50% ACN fraction (**Fig 9A, FigS6D**). We subjected the 50% ACN eluates of ENPP1+ATP and control MCndM to LC-MS analysis, focusing on nucleosides, nucleotides, and their derivatives. We cross checked this list with the mass spectrometry data on the unfractionated ENPP1+ATP conditioned medium to ensure that the compounds were present in the unfractionated ENPP1+ATP MCndM. We chose 7 compounds which were highly enriched in the 50% ACN elutes of the ENPP1+ATP MCndM **(Table 1).** Addition of all 7 compounds to CFs caused severe cell death **(Fig 9B,C)** but addition of uridine together with the 7 compounds rescued cell death **(Fig 9B,C)**. This suggested that the mechanism of cell death following addition of the 7 selected compounds was similar to that mediated by ENPP1+ATP MCndM. Next, we subtracted each compound from the set of 7 compounds to determine which compound was necessary for cell death **(Fig 9D)**. We observed that adenine was the only compound critically necessary for cell death, as removal of adenine resulted in rescue of cell death **(Fig 9D,E)**. However, when CFs were treated with adenine alone, no cell death was observed, demonstrating that adenine though necessary was not sufficient for cell death **(Fig 9F,G)**. We next added adenine plus one of the other 6 compounds and observed that

addition of adenine with either adenosine, inosine or IMP (inosine monophosphate) or AMP was sufficient to cause death (**Fig 9F,G**). Combinations of adenine with either hypoxanthine, xanthine or orotate did not cause cell death **(Fig 9F,G). Finally, a**ddition of OMP or uridine rescued cell death of CFs treated with adenine and adenosine (**Fig 9H,I**). Taken together, these observations demonstrate that the combination of adenine and a purine nucleoside, is sufficient to cause disruption of pyrimidine biosynthesis and induce cell death of non-myocytes and that such cell death can be rescued with pyrimidine supplementation. Addition of adenine and adenosine to macrophages, endothelial cells and smooth muscle cells also induced cell death, demonstrating that a combination of adenine and adenosine could induce cell death on a wide variety of non-myocyte cells **(Fig S6E,F)**.

Next, we wanted to determine whether adenine was a key critical component of the ENPP1+ATP MCndM that induced cell death of non-myocytes. We adopted a loss of function approach to determine whether catabolic removal of adenine would rescue ENPP1+ATP MCndM from causing CF cell death. There is no mammalian enzyme that catabolizes adenine but plants and microorganisms express adenine deaminase which converts adenine to hypoxanthine(28). We lenti-virally expressed yeast adenine deaminase in CFs and immortalized them to create a stable cell line. CFs expressing adenine deaminase were resistant to ENPP1+ ATP MCndM induced cell death (**Fig 9J,K**). These experiments thus conclusively demonstrate that adenine is the key molecule present in ENPP1+ATP MCndM that causes cell death of non-myocytes.

Our data suggests that pyrimidine synthesis is disrupted at the OMP synthesis step. We next investigated potential reasons for the inhibition of OMP synthesis. PRPP

is the donor of phospho-ribose groups for OMP synthesis from orotate as well as in the purine salvage pathway to synthesize AMP from adenine. PRPP synthesis by PRPP synthetase is potently inhibited by AMP and ADP (29). The model illustrated in our findings suggest that the toxicity of the combination of adenine and adenosine could be related to inhibition of PRPP synthetase by AMP with concomitant consumption of PRPP by adenine catalyzed by adenine phosphoribosyl transferase. If so, PRPP levels should be significantly reduced and we observed significantly decreased PRPP levels in CFs treated with ENPP1+ATP MCndM (**Fig S6G**) along with decreased levels of metabolites that are generated using PRPP as a substrate such as NAD with corresponding increase in nicotinamide **(Fig S6H)**.

AMP and not adenosine induces the cardiomyocyte to generate adenine

AMP, a metabolite generated by the hydrolytic activity of ENPP1 on ATP was able to induce the myocyte to secrete pro-apoptotic metabolites. Having identified that adenine is a critical mediator of non-myocyte cell death, we next investigated whether AMP or its metabolite adenosine is needed for the myocyte to secrete pro-apoptotic molecules. Extracellular AMP is hydrolyzed by CD73, a membrane bound protein, to form adenosine. We added AMP to cardiomyocytes in the presence or absence of a CD73 inhibitor, collected the MCndM and subsequently added it CFs (**Fig S7A**). We observed that inhibition of CD73 (using two different inhibitors, AB680, AMP-CP) significantly increased CF cell death, strongly suggesting that AMP and not adenosine is necessary for the cardiomyocytes to secrete pro-apoptotic molecules (**Fig S7A,B**). Conditioned medium from adenosine treated cardiomyocytes (adenosine MCndM) was also unable to induce cell death of CFs (**Fig S7C,D**). Moreover, MCndM collected after the addition

of adenosine receptor agonist NECA did not cause fibroblast cell death (**Fig S7E**). Next, we added ENPP1+ATP to cardiomyocytes in the presence of adenosine receptor antagonists and did not observe any change in the ability of ENPP1+ATP MCndM to cause death of cardiac fibroblasts (**Fig S7F),** corroborating the observation that adenosine was not inducing the cardiomyocyte to secrete pro-apoptotic molecules. Adenosine receptor antagonists also did not affect the ability of cardiomyocytes to remain immune to the ENPP1+ATP MCndM or a combination of adenine and adenosine **(Fig S3D-G).** Finally, we added an adenosine kinase inhibitor (ABT-702) or AMP deaminase inhibitor (cpd3) to cardiomyocytes at the time of addition of AMP. Adenosine kinase inhibitors would decrease the generation of AMP from adenosine, while AMP deaminase inhibitors would increase AMP concentrations by inhibiting AMP deamination. We observed that adenosine kinase inhibitors attenuated cell death of CFs (**Fig S7G,H**) while AMP deaminase inhibitors worsened cell death (**Fig S7I,J**) demonstrating that AMP was critically required by the cardiomyocytes to generate pro-apoptotic molecules.

As cardiomyocyte derived adenine was necessary for non-myocyte cell death, we investigated whether AMP was directly utilized by the cardiac muscle cell for adenine synthesis. For this purpose, we added ENPP1+ N15 labeled ATP (**Fig S8A**) to cardiomyocytes, and treated CFs with the collected MCndM (**Fig S8B**). We then harvested cardiomyocytes treated with ENPP1+N15 labeled ATP, the conditioned medium as well as CFs to determine the fraction of adenine and other key metabolites that would bear the isotope label (**Fig S8B**). The fraction of N15 labeled adenine in the cardiomyocytes was 77% of the total adenine present, while 98% of the adenine in the

conditioned medium and 82% of the adenine in the CFs were labeled (**Fig S8C**). The labeled adenine in the cardiomyocytes contained five 15N atoms, demonstrating direct conversion of 15N5 AMP to adenine by the cardiomyocyte (**Fig S8D**)**.** Also, the majority of the adenine in the conditioned medium had all five nitrogen atoms labeled, demonstrating that adenine synthesized by the cardiomyocyte directly from AMP, is the predominant source of adenine in the conditioned medium (**Fig S8E**). Similarly, the majority of the adenosine, IMP, inosine, and AMP in the cardiomyocyte, conditioned medium, as well as the cardiac fibroblasts was labeled (**Fig S8F**). The fraction of labeled nucleoside guanosine was much lower in the cardiomyocyte, while in the cardiac fibroblasts almost 60% of guanosine was labeled (**Fig S8G**). All four nitrogens in the purine ring of guanosine were 15N, suggesting it was derived from the 15N5 AMP (**Fig S8H**). Labeling of unrelated metabolites such as glutamate, not typically derived from adenosine derivatives was expectedly low demonstrating the fidelity of our system as a negative labeling example (**Fig S8I**).

Taken together these observations demonstrate that AMP formed by ENPP1 mediated hydrolysis of ATP is directly metabolized by the cardiomyocyte to generate adenine and other nucleosides, that are then released extracellularly to exert biological effects.

Uridine administration after heart injury augments cardiac repair and function in vivo.

Uridine supplementation to non-myocytes treated with ENPP1+ATP MCndM rescued cell death. We hypothesized that if ENPP1 worsened cardiac repair by inducing defects in pyrimidine biosynthesis in vivo then administration of uridine should rescue pyrimidine

biosynthesis, and lead to better preservation of post injury cardiac function. We subjected wild type C57BL/6 animals to ischemic cardiac injury and administered uridine by continuous infusion for 14 days starting from the day of injury (**Fig 10A**). Echocardiography demonstrated that uridine significantly preserved post injury cardiac contractile function with a trend towards better preservation of ventricular diameters (**Fig 10B,C**). We observed that 71% of the vehicle injected animals exhibited severe depression in EF compared to only 13% of the animals which received uridine (**Fig 10D, Table S1A**). Histology demonstrated decreased fibrosis in uridine injected animals **(Fig 10E,F).** Approximately 43% of the animals in the vehicle group exhibited severe post infarct fibrosis but none of the animals that received uridine exhibited severe fibrosis (**Fig 10G, Table S1B**). Hearts of uridine injected animals exhibited decreased heart weight/body weight ratios **(Fig 10H) and** significantly increased capillary density (**Fig 10I,J**). These data taken together provide proof of concept that rescue of pyrimidine biosynthesis with pyrimidine supplementation in the injured heart represents a therapeutic strategy for heart repair.

ENPP1 inhibitors as therapeutic agents to enhance wound healing after cardiac injury.

As ENPP1 was the principal nucleotidase in the injured heart, we hypothesized that ENPP1 could serve as a therapeutic target for augmenting cardiac wound healing following ischemic injury. We established a luminescent assay to screen a large library of 200,000 compounds at our institution to identify small molecule inhibitors of ENPP1. Myricetin, a polyphenolic flavonoid(30), was the leading hit with almost 90% inhibition of ENPP1 enzymatic activity and an IC_{50} of 4.8μM (**Fig S9A,B**). Addition of ATP induced

cell death of ENPP1 over-expressing CFs co-cultured with NRVM but concomitant addition of myricetin (10uM) significantly attenuated cell death (**Fig S9C,D**). Next, we treated cardiomyocytes with ENPP1+ATP and myricetin, collected the MCndM, added it to CFs and observed a significant reduction in cell death compared to ENPP1+ATP MCndM (**Fig S9E,F**).

Subsequently, we determined whether administration of myricetin can augment cardiac wound healing in vivo. We subjected C57BL/6 animals to ischemic cardiac injury and administered vehicle or 30mg/kg myricetin intra-peritoneally to the animals starting on the day of injury and continuing daily for 14 days post injury (**Fig 11A**). We harvested the injured hearts following 7 days of myricetin administration and observed significant suppression of ATP hydrolytic activity in the myricetin injected animals (**Fig 11B**). Echocardiography demonstrated significantly better preservation of EF/FS and significantly decreased chamber size in myricetin treated group **(Fig 11C,D)**. More than 66% of the animals in the vehicle injected group had severe heart failure while only 23% of the animals receiving myricetin developed severe heart failure (**Fig 11E, Table S1A**). The area of scarring was also significantly reduced in myricetin treated animals (**Fig 11F,G**). Only 15% of myricetin treated animals developed severe fibrosis in contrast to 56% in the vehicle injected group **(Fig 11H, Table S1B).** Myricetin treated animals exhibited significantly lower heart weight/body weight ratios **(Fig S9G)** and significantly increased capillary density **(Fig S9H,I)**. However, the amount of surviving myocardium 24 hours after injury did not show any significant differences between vehicle and myricetin treated groups (**Fig S9J,K**), suggesting that the effects of ENPP1 inhibition

are likely secondary to enhanced wound healing after cardiac injury rather than on enhanced primary myocyte survival.

Arrest in pyrimidine biosynthesis in non-myocyte cells initiated a DNA damage response with expression of gamma H2A.X and p53Ser15 phosphorylation. We performed immunostaining and observed attenuated expression of gamma H2A.X and p53Ser15 phosphorylation in non-myocyte cells in hearts of myricetin treated animals **(Fig 11I,J).** We confirmed this observation in ENPP1CKO hearts as well. Following injury, a significantly lower number of CFs exhibited gamma H2A.X in ENPP1CKO hearts (**Fig S4O,P**).

Finally, as inhibition of ENPP1 should rescue pyrimidine biosynthesis, we performed metabolomic analysis of injured hearts of myricetin treated animals. Myricetin administration resulted in significant increase in levels of the pyrimidines, uridine and cytidine in the injured regions of the heart and exhibited decrease in carbamoyl phosphate levels compared to vehicle treated injured hearts (**Fig 11K**). As uridine rescues the toxic effects of the combination of adenine and a purine nucleoside, we measured the adenine+adenosine/uridine ratio in cardiac tissue as a metric of cytoxicity and observed that hearts of myricetin treated animals exhibited a decreased cytotoxicity ratio (**Fig 11L**). We also performed metabolomic analysis of the serum and observed orotate to decrease in the serum of myricetin treated animals, while deoxyuridine and orotidine levels increased consistent with rescue of pyrimidine biosynthesis **(Fig 11M).** These in vivo data remarkably mirror our in vitro experiments demonstrating an arrest in pyrimidine biosynthesis at the OMP synthesis step and suggesting the potential use of serum orotidine as a biomarker to monitor wound healing in the heart.

Discussion

Our observations demonstrate a hitherto unappreciated role of the cardiomyocyte in regulating the cardiac repair response by modulating pyrimidine biosynthesis and fates of non-muscle cells. Myocardial necrosis leads to release of extracellular ATP that serves as a DAMP signal. AMP formed by ENPP1 mediated hydrolysis is directly metabolized by the cardiomyocyte to form adenine and other purine nucleosides that are released into the extracellular space. Our isotope labeling experiments suggest that AMP is directly used by the myocyte to generate adenine, and pathways of adenine generation could be related to direct nucleotide phosphorolysis mediated by adenine phosphoribosyl transferase (APRT). The combination of adenine and specific ribonucleosides such as adenosine or inosine exert cytotoxic effects on proliferating non-myocytes by disrupting their pyrimidine biosynthesis. The imbalance of purines/pyrimidines is a key event initiating the cell cycle arrest/apoptotic cascade as supplementation of uridine to correct decreased pyrimidine levels rescues cell death. Myocytes are non-proliferative and although an optimal purine/pyrimidine balance is required for DNA repair in the long term, the non-proliferative state protects the myocyte against cell death resulting from a sudden imbalance of purine/pyrimidine bases after cardiac injury.

Our data suggests an inherent defect in cardiac repair based on the ability of non-proliferative cardiomyocytes to mount a ‘metabolic attack’ and a DNA damage response in proliferative non-myocyte cells, that play a critical role in wound healing. Apoptosis of non-myocytes is known to occur after cardiac injury and confirmed even in human heart samples(31, 32). However, the physiological significance of non-myocyte apoptosis is

unclear. In this regard, our data suggests that there is an optimal balance of fibroblasts, endothelial cells and macrophages required for cardiac repair. Decreased apoptosis of cardiac fibroblasts and endothelial cells in the ENPP1CKO animals was associated with decreased inflammation and led to decreased myofibroblast formation, ECM gene expression and lesser scarring. These data suggest that myofibroblast activation could be regulated by non-myocyte cell death after cardiac injury. The teleological reasons why a cardiac muscle cell would mount such a repair response that ultimately is counterproductive for cardiac healing remain unclear, but such mechanisms of metabolic control could have evolved as a defense response against rapidly proliferating non cardiac cells as in an invading cancer or microbes.

We identified myricetin as a potent inhibitor of ENPP1. Pharmacological targeting of ENPP1 with myricetin in vivo results in rescue of pyrimidine biosynthesis with increased serum orotidine levels suggesting a rescue of OMP synthesis and the potential of using serum orotidine as a biomarker for monitoring disruption in pyrimidine biosynthesis. Although myricetin possesses anti-oxidant and anti-inflammatory properties(33), its ability to inhibit ENPP1 activity in the injured heart along with its rescue of pyrimidine biosynthesis strongly favor a mechanism of benefit based on potent ENPP1 inhibition. In summary, our observations demonstrate a myocyte dependent model of cardiac repair where the cardiac muscle cell by altering the extracellular metabolome regulates biological functions of non-myocyte cells, and plays a pivotal role in determining how the heart heals itself.

Methods

Detailed methods are provided in the Supplemental materials.

Data sets availability

The bulk RNA sequencing and single-cell RNA sequencing in this paper is available at NCBI GEO dataset: GSE185060.

Statistics

All data is presented as mean ± standard error of the mean (SEM), and the value of n represents biological replicates. Statistical analysis was performed using GraphPad (Prism) software using Student's t-test (Two tailed), Ordinary one-way ANOVA with Tukey's multiple comparison test or Ordinary two-way ANOVA with Šídák's multiple comparisons test as appropriate. The chi-square test was used for statistical analysis of contingency tables. A p value <0.05 was considered as statistically significant.

Study approval

All animal studies were approved by the Animal Research Committee, University of California, Los Angeles. All animals were maintained at the UCLA vivarium according to the policies instituted by the American Association for Accreditation of Laboratory Animal Care.

Author contributions

S.L. performed the majority of experiments and data analysis. T.Y. performed echocardiography imaging and analysis in a blinded manner. P.W. performed all surgical procedures. R.W., Y.W., M.N.,Y.Z., performed bench experiments related to cellular and molecular assays of ENPP1. F.M. and M.P. analyzed single cell and bulk RNA-seq data. R.D. and M.J. helped in high through-put ENPP1 assay development and drug discovery. I.G. and K.F. helped in HPLC and analysis. J.H., T.G., U.B., M.S helped in LC-MS runs and analysis. J.L. and M.Seldin performed HMDP analysis. C.R.,

E.A., T.L. performed nucleotide measurements on samples with LC-MS. C.R. also helped design metabolic experiments. S.B. and H.M. assisted in cell cycle analysis. D.T.B. and V.M. provided critical reagents and A.R. maintained colonies and assisted with experiments. D.H. and M.T. performed quantitative phase microscopy experiments. Y-J. L. and P-Y. C. performed traction force microscopy experiments. A.D. conceptualized the project, designed experiments, supervised data collection and analysis, and wrote the manuscript.

Acknowledgments

We thank Dr Andrew Leask, University of Western Ontario, Canada and Dr. Eric Olson, University of Texas Southwestern Medical Center for providing us the Col1a2CreERT and the TCF21MerCreMer mice, respectively. This work was funded by grants from the National Institutes of Health, USA (HL137241, AR075867, HL149687, HL149658, HL152176) and Department of Defense, USA (PR161247, PR190268). The project received additional support from the University of California Center for Accelerated Innovation (UC-CAI), University of California Drug Discovery Consortium (UC-DCC) as well as a research innovation award from the Eli and Edythe Broad Center of Regenerative Medicine and Stem Cell Research, University of California, Los Angeles. VM was supported by an Institute Strategic Program Grant (BB/J004316/1) from the Biotechnology and Biological Sciences Research Council (BBSRC), United Kingdom.

References

1. Antman E, et al. ACC/AHA Guidelines for the Management of Patients With ST-Elevation Myocardial InfarctionA Report of the American College of Cardiology/American Heart Association Task Force on Practice Guidelines (Committee to Revise the 1999 Guidelines for the Management of Patients With Acute Myocardial Infarction). *Journal of the American College of Cardiology.* 2004;44(3):E1-E211.
2. Nahrendorf M, et al. The healing myocardium sequentially mobilizes two monocyte subsets with divergent and complementary functions. *J Exp Med.* 2007;204(12):3037-47.
3. Frangogiannis NG. Emerging roles for macrophages in cardiac injury: cytoprotection, repair, and regeneration. *J Clin Invest.* 2015;125(8):2927-30.
4. Frangogiannis NG. The extracellular matrix in myocardial injury, repair, and remodeling. *J Clin Invest.* 2017;127(5):1600-12.
5. Epelman S, Liu PP, and Mann DL. Role of innate and adaptive immune mechanisms in cardiac injury and repair. *Nat Rev Immunol.* 2015;15(2):117-29.
6. Coade SB, and Pearson JD. Metabolism of adenine nucleotides in human blood. *Circ Res.* 1989;65(3):531-7.
7. Trautmann A. Extracellular ATP in the immune system: more than just a "danger signal". *Sci Signal.* 2009;2(56):pe6.
8. Burnstock G. Purinergic Signaling in the Cardiovascular System. *Circ Res.* 2017;120(1):207-28.
9. Venereau E, Ceriotti C, and Bianchi ME. DAMPs from Cell Death to New Life. *Front Immunol.* 2015;6:422.
10. Kato K, et al. Expression, purification, crystallization and preliminary X-ray crystallographic analysis of Enpp1. *Acta Crystallogr Sect F Struct Biol Cryst Commun.* 2012;68(Pt 7):778-82.
11. Kanisicak O, et al. Genetic lineage tracing defines myofibroblast origin and function in the injured heart. *Nat Commun.* 2016;7:12260.
12. Masse K, Bhamra S, Allsop G, Dale N, and Jones EA. Ectophosphodiesterase/nucleotide phosphohydrolase (Enpp) nucleotidases: cloning, conservation and developmental restriction. *Int J Dev Biol.* 2010;54(1):181-93.
13. Moller S, et al. Monitoring the expression of purinoceptors and nucleotide-metabolizing ecto-enzymes with antibodies directed against proteins in native conformation. *Purinergic Signal.* 2007;3(4):359-66.
14. Yokota T, et al. Type V Collagen in Scar Tissue Regulates the Size of Scar after Heart Injury. *Cell.* 2020.
15. Li Q, Guo H, Chou DW, Berndt A, Sundberg JP, and Uitto J. Mutant Enpp1asj mice as a model for generalized arterial calcification of infancy. *Dis Model Mech.* 2013;6(5):1227-35.
16. Ubil E, et al. Mesenchymal-endothelial transition contributes to cardiac neovascularization. *Nature.* 2014;514(7524):585-90.
17. Acharya A, Baek ST, Banfi S, Eskiocak B, and Tallquist MD. Efficient inducible Cre-mediated recombination in Tcf21 cell lineages in the heart and kidney. *Genesis.* 2011;49(11):870-7.
18. Corriden R, and Insel PA. Basal release of ATP: an autocrine-paracrine mechanism for cell regulation. *Sci Signal.* 2010;3(104):re1.
19. Zangle TA, Burnes D, Mathis C, Witte ON, and Teitell MA. Quantifying biomass changes of single CD8+ T cells during antigen specific cytotoxicity. *PLoS One.* 2013;8(7):e68916.
20. Roberts FL, et al. Osteoblast-specific deficiency of ectonucleotide pyrophosphatase/ phosphodiesterase-1 engenders insulin resistance in high-fat diet fed mice. *Journal of Cell Physiology.* 2020 (In press).

21. Schuleri KH, et al. Cardiovascular magnetic resonance characterization of peri-infarct zone remodeling following myocardial infarction. *Journal of Cardiovascular Magnetic Resonance.* 2012;14(1):24.
22. Rau CD, Lusis AJ, and Wang Y. Systems Genetics for Mechanistic Discovery in Heart Diseases. *Circ Res.* 2020;126(12):1795-815.
23. Rau CD, et al. Mapping Genetic Contributions to Cardiac Pathology Induced by Beta-Adrenergic Stimulation in Mice. *Circ Cardiovasc Genet.* 2014.
24. Nghiem P, Park PK, Kim Ys YS, Desai BN, and Schreiber SL. ATR is not required for p53 activation but synergizes with p53 in the replication checkpoint. *J Biol Chem.* 2002;277(6):4428-34.
25. Canman CE, et al. Activation of the ATM kinase by ionizing radiation and phosphorylation of p53. *Science.* 1998;281(5383):1677-9.
26. Marino S, Vooijs M, van Der Gulden H, Jonkers J, and Berns A. Induction of medulloblastomas in p53-null mutant mice by somatic inactivation of Rb in the external granular layer cells of the cerebellum. *Genes Dev.* 2000;14(8):994-1004.
27. Pai CC, and Kearsey SE. A Critical Balance: dNTPs and the Maintenance of Genome Stability. *Genes (Basel).* 2017;8(2).
28. Deeley MC. Adenine deaminase and adenine utilization in Saccharomyces cerevisiae. *J Bacteriol.* 1992;174(10):3102-10.
29. Switzer RL, and Sogin DC. Regulation and mechanism of phosphoribosylpyrophosphate synthetase. V. Inhibition by end products and regulation by adenosine diphosphate. *J Biol Chem.* 1973;248(3):1063-73.
30. Ong KC, and Khoo HE. Biological effects of myricetin. *Gen Pharmacol.* 1997;29(2):121-6.
31. Ivey MJ, Kuwabara JT, Pai JT, Moore RE, Sun Z, and Tallquist MD. Resident fibroblast expansion during cardiac growth and remodeling. *J Mol Cell Cardiol.* 2018;114:161-74.
32. Park M, et al. Apoptosis predominates in nonmyocytes in heart failure. *Am J Physiol Heart Circ Physiol.* 2009;297(2):H785-91.
33. Semwal DK, Semwal RB, Combrinck S, and Viljoen A. Myricetin: A Dietary Molecule with Diverse Biological Activities. *Nutrients.* 2016;8(2):90.

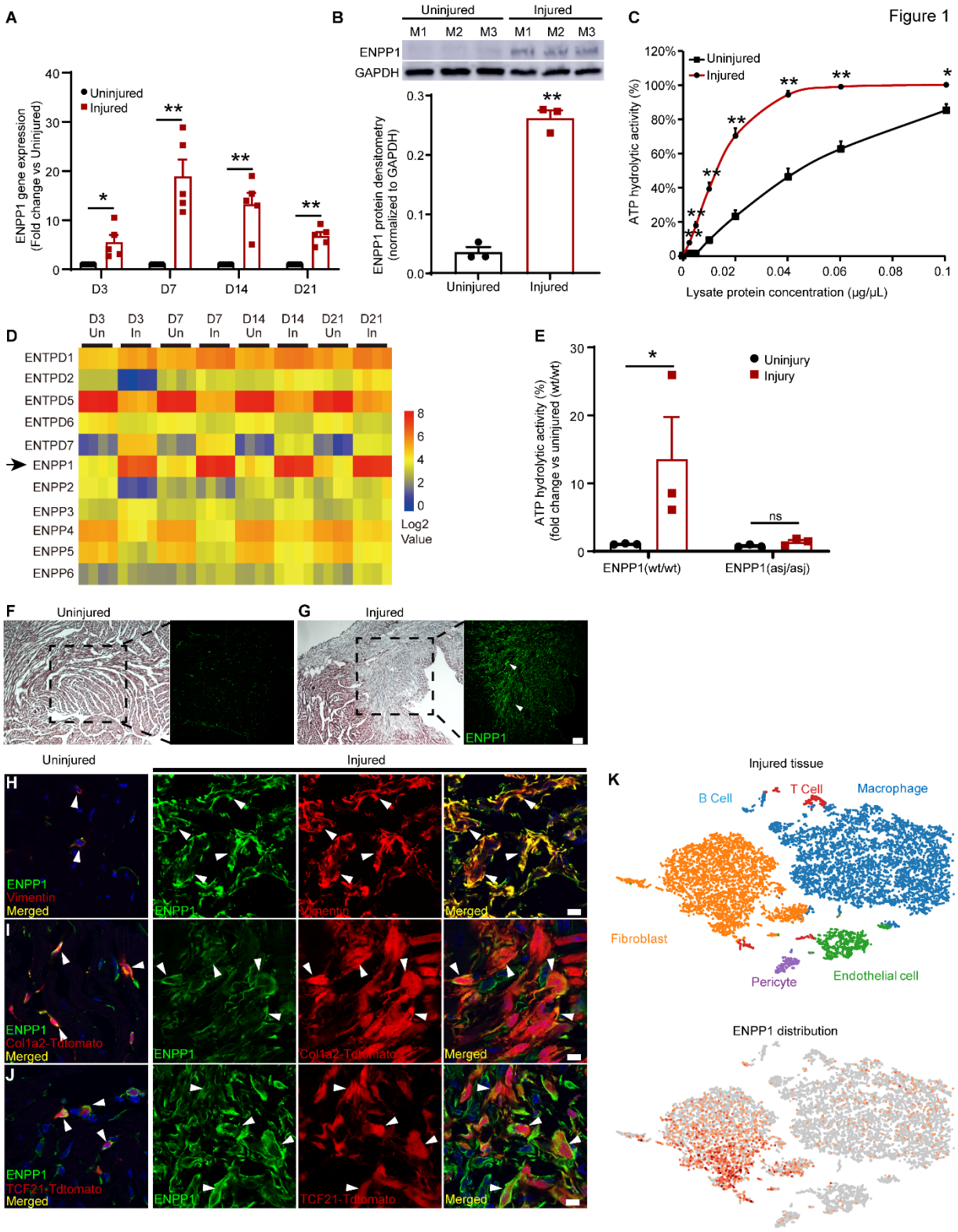
Figure 1
A
ENPP1 gene expression (Fold change vs Uninjured)
Uninjured
Injured
D3
D7
D14
D21
B
Uninjured
Injured
M1
M2
M3
ENPP1
GAPDH
ENPP1 protein densitometry (normalized to GAPDH)
C
ATP hydrolytic activity (%)
Lysate protein concentration (μg/μL)
D
ENTPD1
ENTPD2
ENTPD5
ENTPD6
ENTPD7
ENPP1
ENPP2
ENPP3
ENPP4
ENPP5
ENPP6
Log2 Value
E
ATP hydrolytic activity (%) (fold change vs uninjured (wt/wt)
Uninjury
Injury
ENPP1(wt/wt)
ENPP1(asj/asj)
ns
F
Uninjured
G
Injured
ENPP1
H
ENPP1
Vimentin
Merged
I
ENPP1
Col1a2-Tdtomato
Merged
J
ENPP1
TCF21-Tdtomato
Merged
K
Injured tissue
B Cell
T Cell
Macrophage
Fibroblast
Pericyte
Endothelial cell
ENPP1 distribution

Figure 1. ENPP1 is expressed in the infarcted heart by non-myocytes and is the principal ectonucleotidase that hydrolyzes extracellular ATP. (A) qPCR demonstrating ENPP1 gene expression in the injured region of the heart compared to uninjured regions at 3, 7, 14 and 21 days after MI (n=5). **(B)** Western blotting and quantitative densitometry demonstrating ENPP1 protein level in injured and uninjured regions of the heart at 7 days following MI (n=3). **(C)** ATP hydrolytic activity at various concentrations of the injured heart tissue homogenate compared to uninjured tissue homogenate 7 days after MI (n=3). **(D)** Heatmap with gene expression patterns of ENPP1 (arrow) and other members of the ENPP and ectonucleotidase family in the injured versus uninjured regions of the heart (n=4/time point, Un:Uninjured & In:Injured tissue). **(E)** ATP hydrolytic activity at 7 days post MI in wild type mice and $ENPP1^{asj/asj}$ mutant mice (n=3). **(F,G)** Hematoxylin & eosin stain and immunostaining for ENPP1 (green, arrows) in the uninjured **(F)** and injured **(G)** regions at day 7 post MI. Scale Bar: 100 μm. **(H)** Immunostaining for ENPP1 and Vimentin in the uninjured and injured region at 7 days post MI (arrowheads indicate ENPP1 and Vimentin colocalization in merged image). **(I,J)** Immunostaining of ENNP1 expression in genetically labeled cardiac fibroblasts in **(I)** Col1a2CreERT:$R26R^{tdtomato}$ or **(J)** TCF21MCM:$R26R^{tdtomato}$ mice at 7 days post MI (arrowheads indicate where ENPP1 expressing cells co-express the fibroblast tdTomato label, representative images, n=3). Scale Bar: 10 μm. **(K)** Single cell RNA-seq of non-myocytes at 7 days post MI demonstrating cell phenotypes in clusters and ENPP1 distribution (n=3). Data are expressed as mean ± S.E.M. $^{**}p<0.01$, $^{*}p<0.05$, ns: not significant, Statistics was determined using Student's t-test, 2 tailed **(A, B, C, E)**

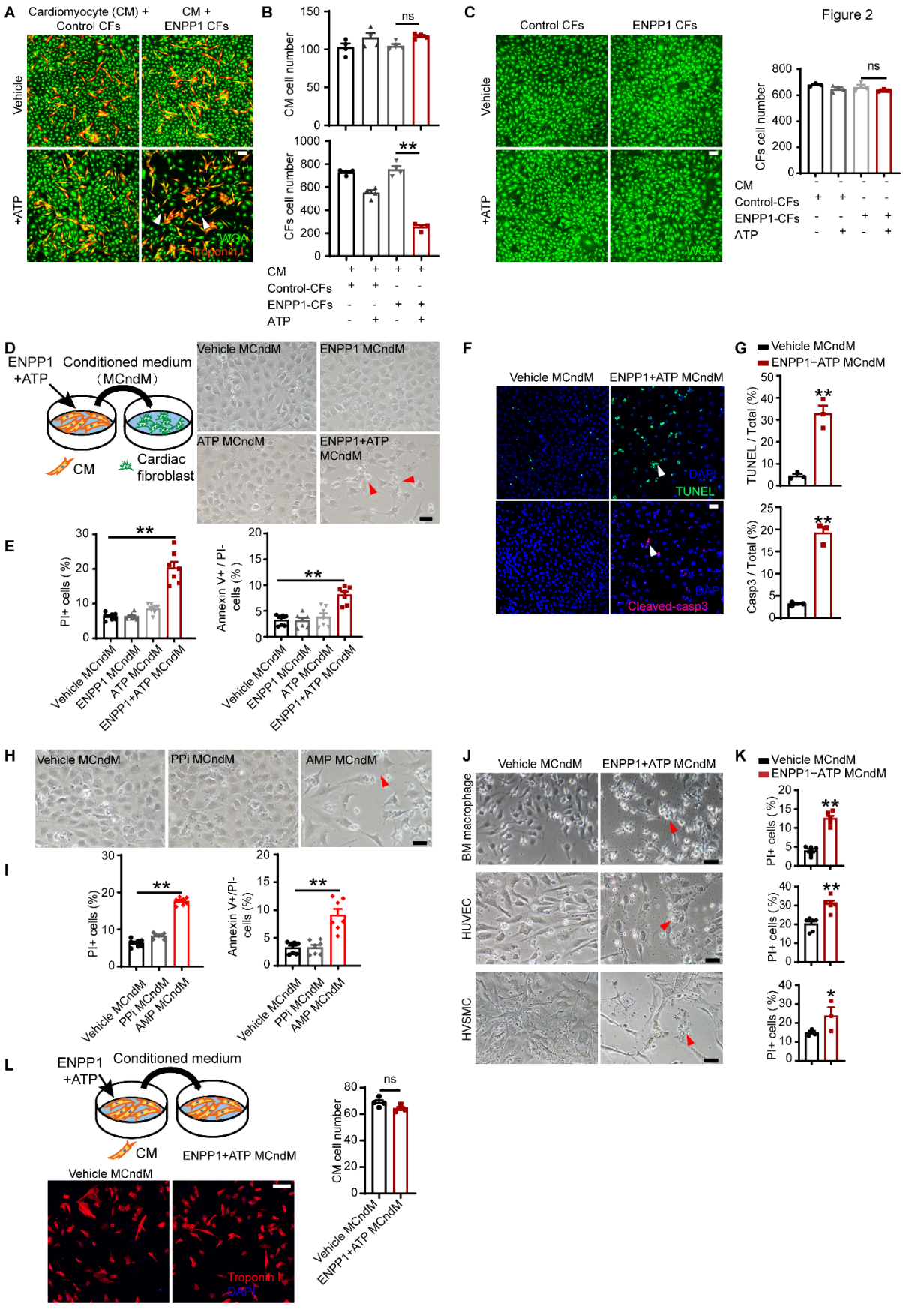
Figure 2
A
Cardiomyocyte (CM) + Control CFs
CM + ENPP1 CFs
Vehicle
+ATP
WGA
Troponin I
B
CM cell number
CFs cell number
ns
**
CM
Control-CFs
ENPP1-CFs
ATP
C
Control CFs
ENPP1 CFs
Vehicle
+ATP
WGA
CFs cell number
ns
CM
Control-CFs
ENPP1-CFs
ATP
D
ENPP1 +ATP
Conditioned medium (MCndM)
CM
Cardiac fibroblast
Vehicle MCndM
ENPP1 MCndM
ATP MCndM
ENPP1+ATP MCndM
E
PI+ cells (%)
Annexin V+ / PI- cells (%)
**
Vehicle MCndM
ENPP1 MCndM
ATP MCndM
ENPP1+ATP MCndM
F
Vehicle MCndM
ENPP1+ATP MCndM
DAPI
TUNEL
Cleaved-casp3
G
Vehicle MCndM
ENPP1+ATP MCndM
TUNEL / Total (%)
Casp3 / Total (%)
**
H
Vehicle MCndM
PPi MCndM
AMP MCndM
I
PI+ cells (%)
Annexin V+/PI- cells (%)
**
Vehicle MCndM
PPi MCndM
AMP MCndM
J
Vehicle MCndM
ENPP1+ATP MCndM
BM macrophage
HUVEC
HVSMC
K
Vehicle MCndM
ENPP1+ATP MCndM
PI+ cells (%)
**
*
L
ENPP1 +ATP
Conditioned medium
CM
ENPP1+ATP MCndM
Vehicle MCndM
Troponin I
DAPI
CM cell number
ns
Vehicle MCndM
ENPP1+ATP MCndM

Figure 2. ENPP1 in the presence of ATP induces the cardiomyocyte to release pro-apoptotic molecules. (A) Co-culture of rat ventricular cardiomyocytes (CMs, red) with Control or ENPP1 overexpressing cardiac fibroblasts (Control-CF, ENPP1-CF, green) with/without ATP (arrows show decrease in ENPP1-CF). Scale Bar: 100 μm. **(B)** Number of CMs and cardiac fibroblasts following 48 hours of co-culture (n=4). **(C)** Control CFs or ENPP1 CFs (green) in the presence or absence of added ATP but without any cardiomyocytes, and quantitation of cell numbers after 48 hours of ATP/vehicle addition (n=3). Scale Bar: 100 μm. **(D)** Transfer of control or ENPP1+ATP myocyte conditioned medium (MCndM) to CFs and images 48 hours later demonstrating decreased number of CF treated with ENPP1+ATP MCndM (arrows). Scale Bar: 50 μm. **(E)** Flow cytometry to demonstrate the fraction of dead (PI+) or apoptotic cells (Annexin V+, PI-) following treatment with ENPP1+ATP MCndM or control MCndM (n=7). **(F)** TUNEL and caspase staining of CFs treated with vehicle MCndM or ENPP1+ATP MCndM and **(G)** quantitation (n=3). Scale Bar: 50 μm. **(H)** CFs treated with Vehicle MCndM, PPi MCndM or AMP MCndM for 48 hours showing loss of cells with treatment with AMP MCndM (arrow) and **(I)** quantitation of dead cells (n=7). Scale Bar: 50 μm. **(J)** Treatment of macrophages, human endothelial (HUVEC) and human vascular smooth muscle cells (hVSMC) with vehicle MCndM or ENPP1+ATP MCndM and **(K)** corresponding flow cytometry to determine cell death (n=6/6/3 for BM macrophage/HUVEC/HVSMC). Scale Bar: 50 μm. **(L)** ENPP1+ATP MCndM does not cause cell death when added to myocytes (n=4). Scale Bar: 100 μm. Data are expressed as mean ± S.E.M. **p<0.01, *p<0.05, ns: not significant, Statistics was determined using Ordinary one-way ANOVA with Tukey's multiple comparison test **(B, C, E, I)** or Student's t-test, 2 tailed **(G, K, L).**

Figure 3

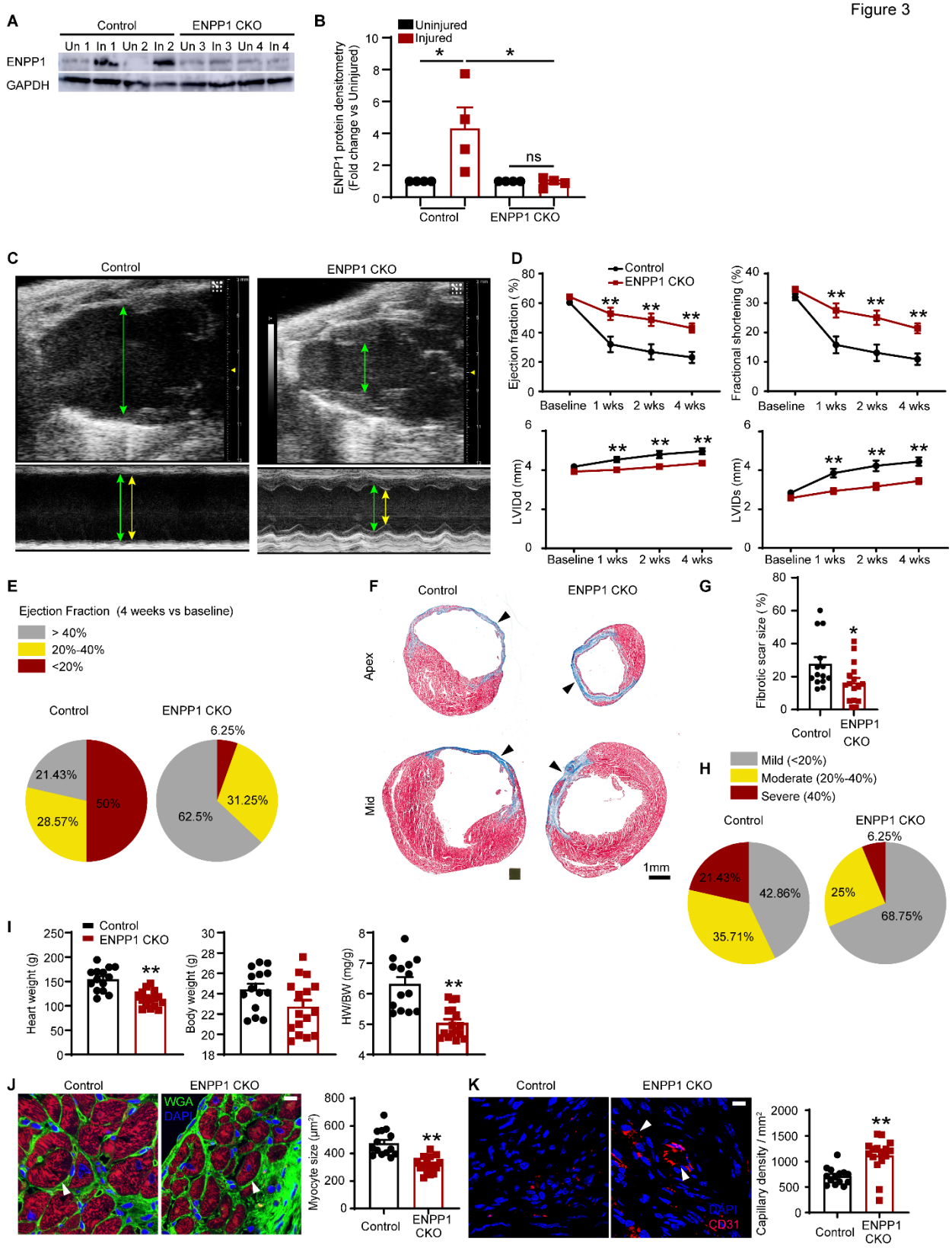
A
Control
ENPP1 CKO
Un 1 In 1 Un 2 In 2 Un 3 In 3 Un 4 In 4
ENPP1
GAPDH
B
Uninjured
Injured
ENPP1 protein densitometry (Fold change vs Uninjured)
*
*
ns
Control
ENPP1 CKO
C
Control
ENPP1 CKO
D
Control
ENPP1 CKO
Ejection fraction (%)
Fractional shortening (%)
LVIDd (mm)
LVIDs (mm)
Baseline 1 wks 2 wks 4 wks
**
E
Ejection Fraction (4 weeks vs baseline)
> 40%
20%-40%
<20%
Control
ENPP1 CKO
21.43%
50%
28.57%
6.25%
31.25%
62.5%
F
Control
ENPP1 CKO
Apex
Mid
1mm
G
Fibrotic scar size (%)
Control
ENPP1 CKO
H
Mild (<20%)
Moderate (20%-40%)
Severe (40%)
Control
ENPP1 CKO
21.43%
42.86%
35.71%
6.25%
25%
68.75%
I
Control
ENPP1 CKO
Heart weight (g)
Body weight (g)
HW/BW (mg/g)
**
J
Control
ENPP1 CKO
WGA
DAPI
Myocyte size (μm²)
Control
ENPP1 CKO
K
Control
ENPP1 CKO
DAPI
CD31
Capillary density / mm²
Control
ENPP1 CKO

Figure 3. Genetic deletion of ENPP1 leads to enhanced cardiac repair and better preservation of post injury heart function. (A) Western blotting for ENPP1 expression in the hearts of ENPP1CKO animals at 7 days following cardiac injury and **(B)** quantitative densitometry of ENPP1 expression (n=4). **(C)** B mode and M mode echocardiogram demonstrating better contractile function with decreased chamber dilatation at 4 weeks following cardiac injury (green arrow: diastole; yellow arrow: systole). **(D)** Ejection fraction and Fractional shortening as well as left ventricular chamber size (LVID) in systole (s) and diastole (d) over 4 weeks after cardiac injury in control and ENPP1CKO animals. **(E)** Pie chart demonstrating fraction of animals with mild, moderate and severe reductions in EF. **(F)** Masson trichrome staining demonstrating scar size (blue) measured at the apex and mid ventricle and **(G)** quantitation of differences in scar size as a fraction of the left ventricular surface area. **(H)** Pie chart showing animals (%) with mild, moderate and severe fibrosis **(I)** Heart weight (HW), body weight (BW) and HW/BW ratios measured at 4 weeks following cardiac injury and **(J)** Cardiac troponin T immunostaining to determine myocyte surface area (arrows) at the border zone and quantitation of myocyte surface area. Scale Bar: 10 μm. **(K)** number of capillaries (CD31 staining, arrows) in ENPP1CKO and control animals at 4 weeks after heart injury and quantitation of capillary density. Scale Bar: 10 μm. Data are expressed as mean ± S.E.M. **p<0.01, *p<0.05, ns: not significant, Statistics was determined using Ordinary one-way ANOVA with Tukey's multiple comparison test **(B),** Ordinary two-way ANOVA with Šídák's multiple comparisons test **(D)** or Student's t-test, 2 tailed **(G, I, J, K).** n=14 in control and n=16 in ENPP1CKO animals **(D, E, G, H, I, J, K).**

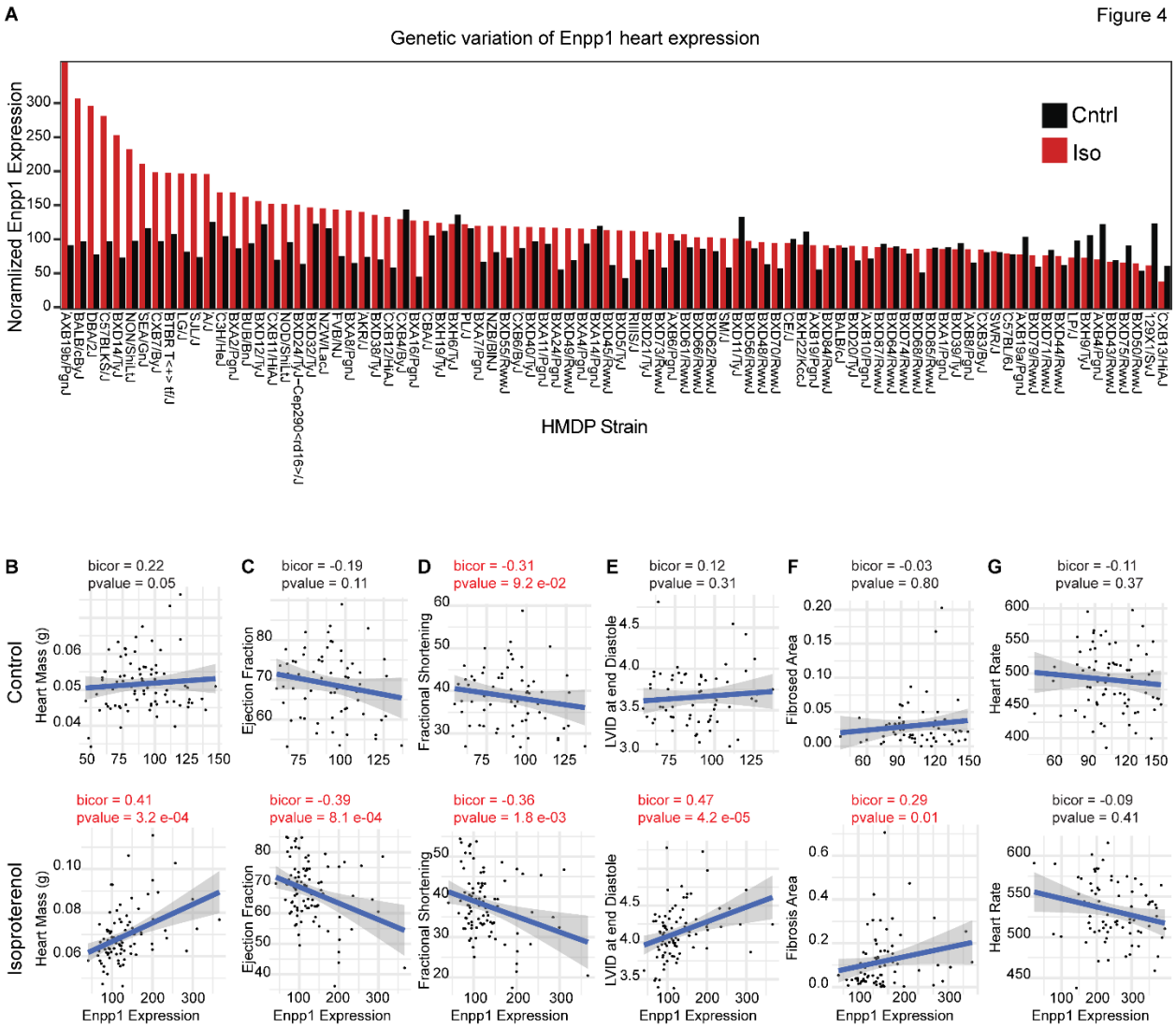

Figure 4. ENPP1 expression across 100 strains of mice correlates with cardiac function in an isoproterenol induced cardiac injury model (A) Genetic variation of ENPP1 expression across 100 strains of mice following 3 weeks of isoproterenol or saline (control) infusion **(B-F)** Cardiac traits of **(B)** cardiac mass and **(C)** ejection fraction **(D)** fractional shortening **(E)** Left ventricular chamber size (LVID(d) and **(F)** Fibrosis strongly correlating with ENPP1 expression across 100 strains of mice while **(G)** there is an absence of correlation with a trait such as heart rate. Data shown as scatterplots. Bicor = midweight bicorrelation coefficient and corresponding regression students p value.

Figure 5

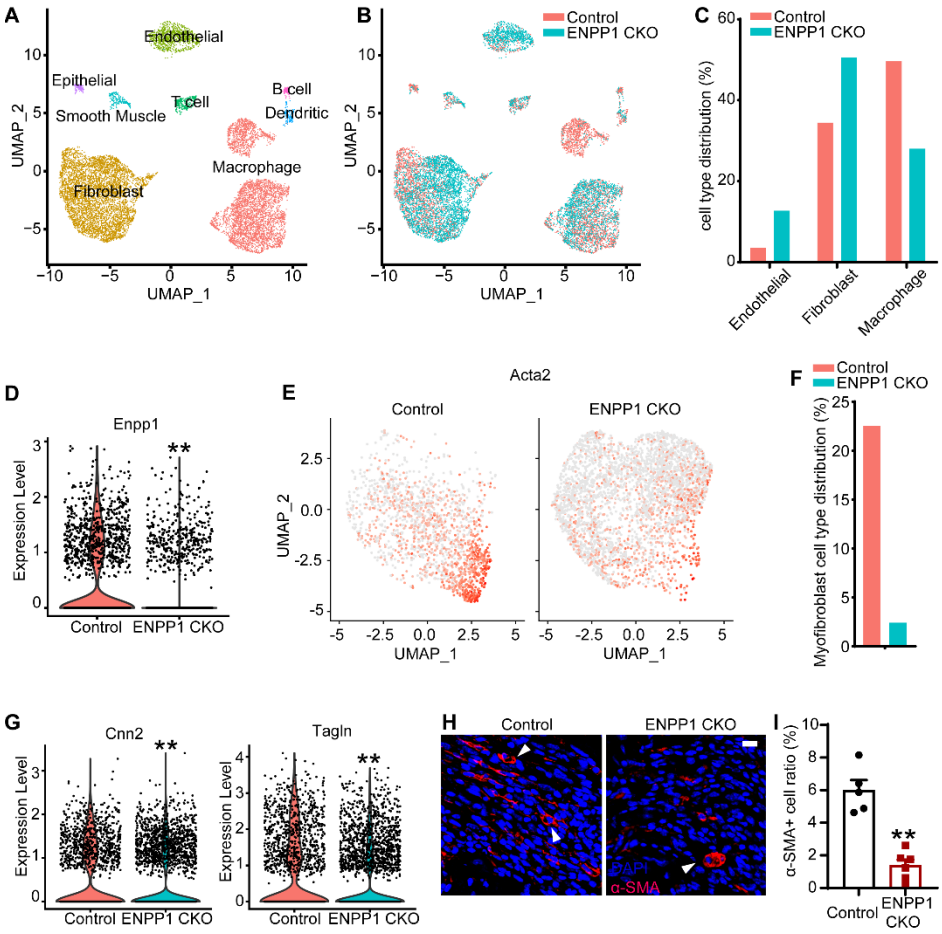

Figure 5. Single cell RNA-seq of non-myocytes in control and ENPP1CKO animals at 7 days following cardiac injury. (A) UMAP demonstrating different phenotypes of non-myocyte cell clusters in the injured heart and **(B)** distribution of WT and ENPP1CKO cells across these clusters. **(C)** Fraction of endothelial cell, fibroblasts and macrophages at 7 days following injury. Violin plot demonstrating **(D)** ENPP1 expression (**p=5.29e-132) and **(E)** UMAP demonstrating significantly reduced distribution of Acta2 (myofibroblast marker) in cardiac fibroblasts of ENPP1CKO versus control animals and **(F)** quantitation (%) of myofibroblasts (**G**) Violin plot demonstrating decreased expression of other myofibroblast genes Cnn2 (**p=3.63e-24) and Tagln (**p=5.40e-17) in ENPP1CKO fibroblasts **(H)** Immunostaining for myofibroblasts (αSMA expression) in ENPP1CKO and WT animals and **(I)** quantitation of myofibroblast numbers (mean ± S.E.M. n=5, **p<0.01, Student's t-test, 2 tailed) Scale Bar: 10 μm.

Figure 6

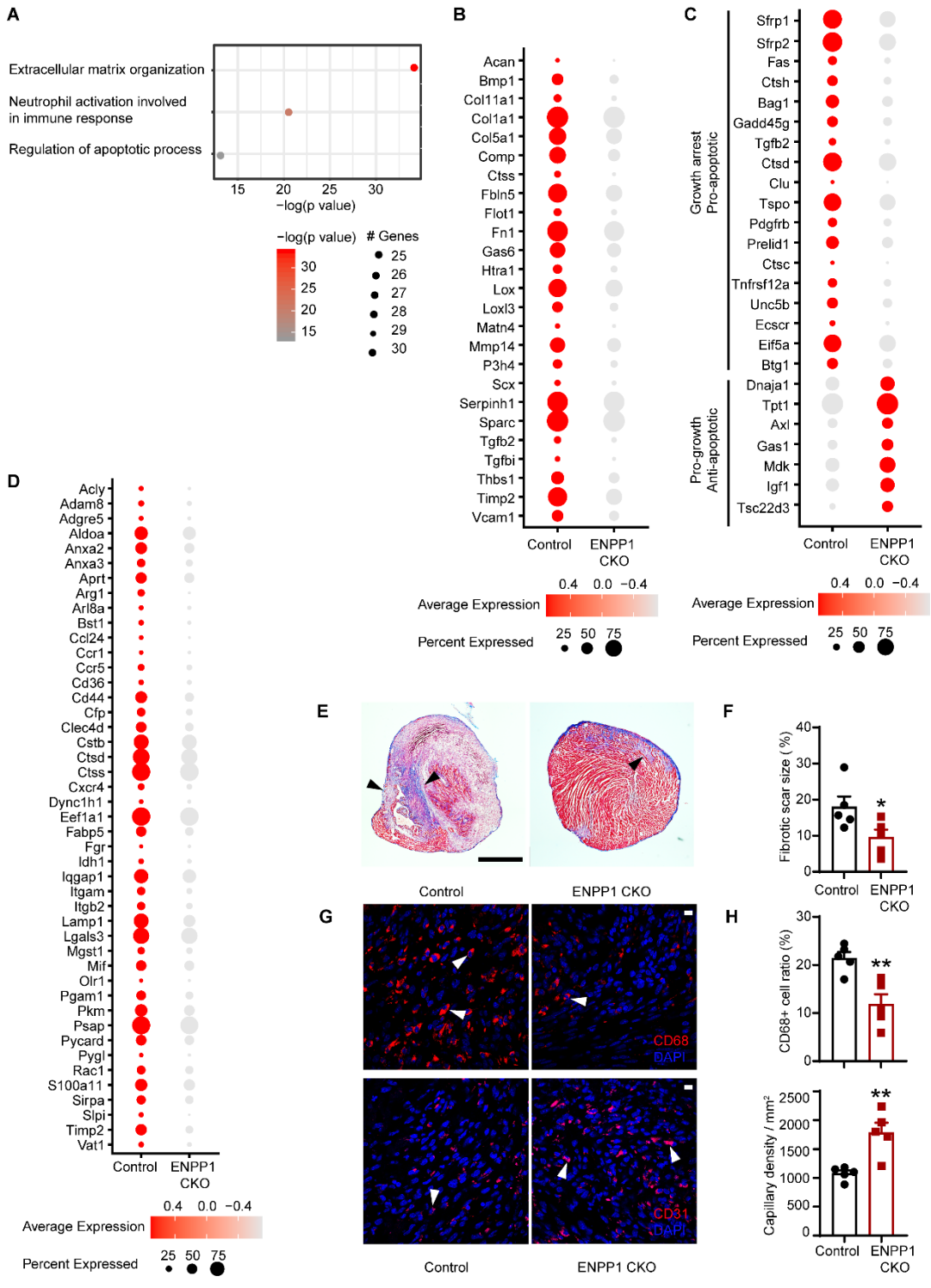
A
Extracellular matrix organization
Neutrophil activation involved in immune response
Regulation of apoptotic process
15 20 25 30
−log(p value)
−log(p value)
30 25 20 15
Genes
25 26 27 28 29 30
B
Acan Bmp1 Col11a1 Col1a1 Col5a1 Comp Ctss Fbln5 Flot1 Fn1 Gas6 Htra1 Lox Loxl3 Matn4 Mmp14 P3h4 Scx Serpinh1 Sparc Tgfb2 Tgfbi Thbs1 Timp2 Vcam1
Control ENPP1 CKO
Average Expression
0.4 0.0 −0.4
Percent Expressed
25 50 75
C
Growth arrest Pro-apoptotic
Sfrp1 Sfrp2 Fas Ctsh Bag1 Gadd45g Tgfb2 Ctsd Clu Tspo Pdgfrb Prelid1 Ctsc Tnfrsf12a Unc5b Ecscr Eif5a Btg1
Pro-growth Anti-apoptotic
Dnaja1 Tpt1 Axl Gas1 Mdk Igf1 Tsc22d3
Control ENPP1 CKO
Average Expression
0.4 0.0 −0.4
Percent Expressed
25 50 75
D
Acly Adam8 Adgre5 Aldoa Anxa2 Anxa3 Aprt Arg1 Arl8a Bst1 Ccl24 Ccr1 Ccr5 Cd36 Cd44 Cfp Clec4d Cstb Ctsd Ctss Cxcr4 Dync1h1 Eef1a1 Fabp5 Fgr Idh1 Iqgap1 Itgam Itgb2 Lamp1 Lgals3 Mgst1 Mif Olr1 Pgam1 Pkm Psap Pycard Pygl Rac1 S100a11 Sirpa Slpi Timp2 Vat1
Control ENPP1 CKO
Average Expression
0.4 0.0 −0.4
Percent Expressed
25 50 75
E
Control
ENPP1 CKO
F
Fibrotic scar size (%)
40 30 20 10 0
*
Control ENPP1 CKO
G
Control
ENPP1 CKO
CD68
DAPI
CD31
DAPI
Control
ENPP1 CKO
H
CD68+ cell ratio (%)
30 20 10 0
**
Capillary density / mm²
2500 2000 1500 1000 500 0
**
Control ENPP1 CKO

Figure 6. GO analysis of non-myocyte single cell RNA-seq at 7 days following cardiac injury. (**A**) GO analysis demonstrating principal pathways upregulated in CFs of control mice versus ENPP1CKO animals **(B)** Dot-plot demonstrating principal ECM genes upregulated in control versus ENPP1CKO CFs 7 days after cardiac injury **(C)** Dot plot demonstrating differential expression of pro and anti-apoptotic genes in CFs at 7 days post injury **(D)** Dot plot demonstrating differential expression of inflammatory genes in macrophages of control and ENPP1CKO hearts at 7 days post injury **(E)** Masson trichrome staining showing expression of collagen (blue) in the apical region of hearts of mice at 7 days following injury and **(F)** quantitation of fibrotic scar size at 7 days following injury (n=5) Scale Bar: 1 mm. **(G)** Immunofluorescent staining demonstrating CD68 (macrophages) and CD31 (endothelial) staining in control and ENPP1CKO animals at 7 days following injury and **(H)** quantitation of cells by histology (n=5). Scale Bar: 10 μm. Data are expressed as mean ± S.E.M. **p<0.01, *p<0.05, Statistics was determined using Student's t-test, 2 tailed **(F, H).**

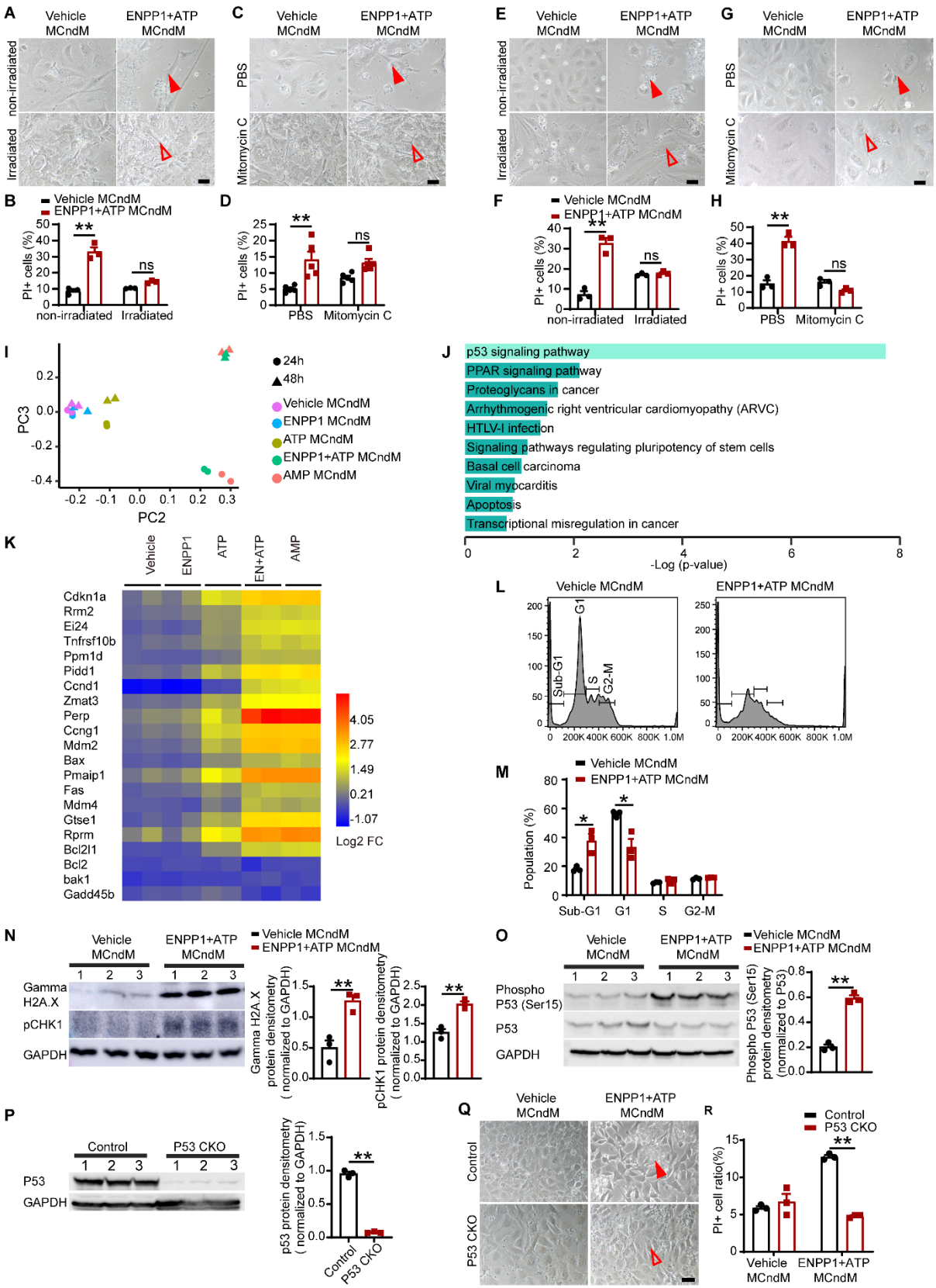
A
Vehicle MCndM
ENPP1+ATP MCndM
non-irradiated
Irradiated
B
Vehicle MCndM
ENPP1+ATP MCndM
PI+ cells (%)
**
ns
non-irradiated
Irradiated
C
Vehicle MCndM
ENPP1+ATP MCndM
PBS
Mitomycin C
D
PI+ cells (%)
**
ns
PBS
Mitomycin C
E
Vehicle MCndM
ENPP1+ATP MCndM
non-irradiated
Irradiated
F
Vehicle MCndM
ENPP1+ATP MCndM
PI+ cells (%)
**
ns
non-irradiated
Irradiated
G
Vehicle MCndM
ENPP1+ATP MCndM
PBS
Mitomycin C
H
PI+ cells (%)
**
ns
PBS
Mitomycin C
I
24h
48h
Vehicle MCndM
ENPP1 MCndM
ATP MCndM
ENPP1+ATP MCndM
AMP MCndM
PC3
PC2
J
p53 signaling pathway
PPAR signaling pathway
Proteoglycans in cancer
Arrhythmogenic right ventricular cardiomyopathy (ARVC)
HTLV-I infection
Signaling pathways regulating pluripotency of stem cells
Basal cell carcinoma
Viral myocarditis
Apoptosis
Transcriptional misregulation in cancer
-Log (p-value)
K
Vehicle
ENPP1
ATP
EN+ATP
AMP
Cdkn1a
Rrm2
Ei24
Tnfrsf10b
Ppm1d
Pidd1
Ccnd1
Zmat3
Perp
Ccng1
Mdm2
Bax
Pmaip1
Fas
Mdm4
Gtse1
Rprm
Bcl2l1
Bcl2
bak1
Gadd45b
4.05
2.77
1.49
0.21
-1.07
Log2 FC
L
Vehicle MCndM
ENPP1+ATP MCndM
G1
S
G2-M
Sub-G1
M
Vehicle MCndM
ENPP1+ATP MCndM
Population (%)
Sub-G1
G1
S
G2-M
N
Vehicle MCndM
ENPP1+ATP MCndM
Gamma H2A.X
pCHK1
GAPDH
Gamma H2A.X protein densitometry (normalized to GAPDH)
pCHK1 protein densitometry (normalized to GAPDH)
O
Vehicle MCndM
ENPP1+ATP MCndM
Phospho P53 (Ser15)
P53
GAPDH
Phospho P53 (Ser15) protein densitometry (normalized to P53)
P
Control
P53 CKO
P53
GAPDH
p53 protein densitometry (normalized to GAPDH)
Q
Vehicle MCndM
ENPP1+ATP MCndM
Control
P53 CKO
R
Control
P53 CKO
PI+ cell ratio(%)
Vehicle MCndM
ENPP1+ATP MCndM

Figure 7. Pro-apoptotic molecules secreted by cardiomyocytes cause cell death only in cycling cells (A) Irradiated or non-irradiated CFs treated with vehicle or ENPP1+ATP MCndM for 48 hours. Cell death in irradiated but not in irradiated CF (unfilled arrow) **(B)** Quantitation of cell death (n=3). (**C)** PBS or mitomycin C treated CFs treated with vehicle or ENPP1+ATP MCndM for 48 hrs; rescue of cell death with mitomycin (filled and unfilled arrows) **(D)** Quantitation of cell death (n=5). Scale Bar: 50 μm. **(E-H)** MEFs treated with Vehicle or ENPP1+ATP MCndM following **(E)** irradiation or **(G)** mitomycin C. Rescue of cell death with irradiation or mitomycin C (filled and unfilled arrows) and **(F,H)** Quantification of cell death following **(F)** irradiation (n=3) or **(H)** mitomycin treatment (n=3). Scale Bar: 50 μm. **(I)** Principal component analysis of gene expression changes in CFs treated with ENPP1+ATP MCndM (n=2). **(J)** GO analysis of main differentially expressed pathways in CFs following treatment with ENPP1+ATP MCndM. **(K)** Heat map demonstrating expression of p53 driven apoptotic genes in CFs treated with ENPP1+ATP MCndM. **(L)** Cell cycle analysis demonstrating G1/S phase arrest in CFs treated with ENPP1+ATP MCndM and **(M)** Cells (%) in different phases of cell cycle (n=3). **(N)** WB for pH2A.X and pCHK-1 in CF treated with ENPP1+ATP MCndM (n=3). **(O)** WB and densitometry of p53 Ser15 phosphorylation in CF treated with ENPP1+ ATP MCndM (n=3). **(P)** p53 protein levels in p53CKO CFs (n=3) **(Q)** p53CKO CFs treated with vehicle or ENPP1 MCndM demonstrating rescue of cell death in p53CKO CFs (filled and unfilled arrows) and **(R)** quantitation of cell death (n=3). Scale Bar: 50 μm. Data are expressed as mean ± S.E.M. **p<0.01, *p<0.05, ns: not significant, Statistics was determined using Student's t-test, 2 tailed **(B, D, F, H, M, N, O, P, R).**

Figure 8

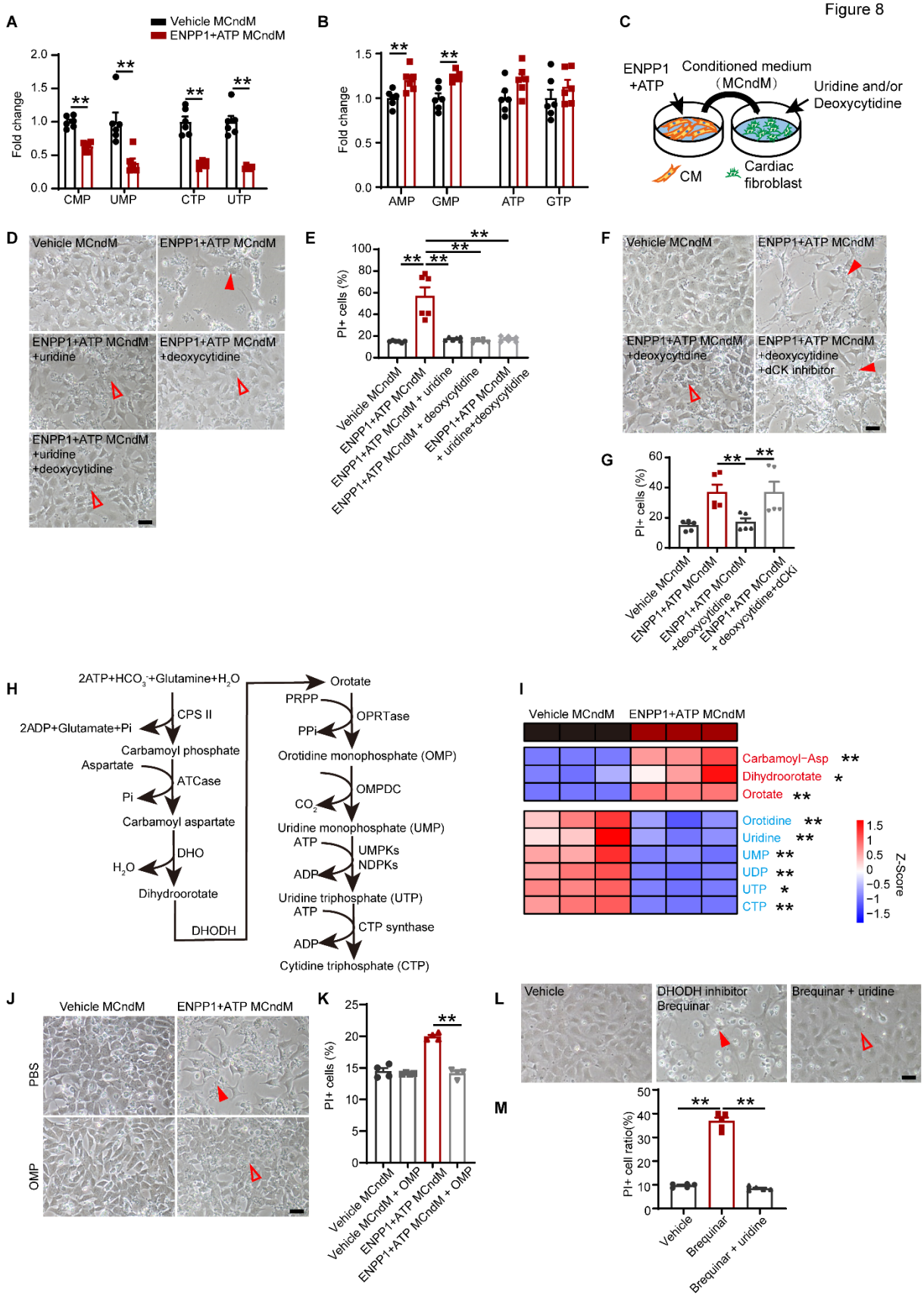
A
Vehicle MCndM
ENPP1+ATP MCndM
Fold change
CMP
UMP
CTP
UTP
B
Fold change
AMP
GMP
ATP
GTP
C
ENPP1 +ATP
Conditioned medium (MCndM)
Uridine and/or Deoxycytidine
CM
Cardiac fibroblast
D
Vehicle MCndM
ENPP1+ATP MCndM
ENPP1+ATP MCndM +uridine
ENPP1+ATP MCndM +deoxycytidine
ENPP1+ATP MCndM +uridine +deoxycytidine
E
PI+ cells (%)
Vehicle MCndM
ENPP1+ATP MCndM
ENPP1+ATP MCndM + uridine
ENPP1+ATP MCndM + deoxycytidine
ENPP1+ATP MCndM + uridine+deoxycytidine
F
Vehicle MCndM
ENPP1+ATP MCndM
ENPP1+ATP MCndM +deoxycytidine
ENPP1+ATP MCndM +deoxycytidine +dCK inhibitor
G
PI+ cells (%)
Vehicle MCndM
ENPP1+ATP MCndM
ENPP1+ATP MCndM +deoxycytidine
ENPP1+ATP MCndM + deoxycytidine+dCKi
H
2ATP+HCO3-+Glutamine+H2O
CPS II
2ADP+Glutamate+Pi
Carbamoyl phosphate
Aspartate
ATCase
Pi
Carbamoyl aspartate
DHO
H2O
Dihydroorotate
DHODH
Orotate
PRPP
OPRTase
PPi
Orotidine monophosphate (OMP)
OMPDC
CO2
Uridine monophosphate (UMP)
ATP
UMPKs NDPKs
ADP
Uridine triphosphate (UTP)
ATP
CTP synthase
ADP
Cytidine triphosphate (CTP)
I
Vehicle MCndM
ENPP1+ATP MCndM
Carbamoyl−Asp
Dihydroorotate
Orotate
Orotidine
Uridine
UMP
UDP
UTP
CTP
Z-Score
J
Vehicle MCndM
ENPP1+ATP MCndM
PBS
OMP
K
PI+ cells (%)
Vehicle MCndM
Vehicle MCndM + OMP
ENPP1+ATP MCndM
ENPP1+ATP MCndM + OMP
L
Vehicle
DHODH inhibitor Brequinar
Brequinar + uridine
M
PI+ cell ratio(%)
Vehicle
Brequinar
Brequinar + uridine

Figure 8. Cardiac fibroblasts treated with ENPP1+ATP (MCndM) exhibit decreased pyrimidine levels. (A) LC/MS-MS demonstrating decreased levels of intracellular pyrimidine nucleotides but not **(B)** purine nucleotides in CFs treated with ENPP1+ATP MCndM (n=6). **(C)** CFs treated with vehicle MCndM or ENPP1+ATP MCndM in the presence of uridine, deoxycytidine or both demonstrating **(D)** cell death (arrows) in CFs treated with ENPP1+ATP MCndM but rescue of cell death (unfilled arrows) following addition of uridine, deoxycytidine or both. Scale Bar: 50 μm. **(E)** Flow cytometry to demonstrate effects on cell death following addition of uridine or deoxycytidine to CFs treated with ENPP1+ATP MCndM (n=6). **(F)** Effect of adding deoxycytidine and deoxycytidine kinase inhibitor (dCKi) to CFs treated with ENPP1+ATP MCndM demonstrates loss of rescue of deoxycytidine in the presence of dCKi (unfilled and filled arrows) and **(G)** quantitation of cell death (n=5). Scale Bar: 50 μm. **(H)** Outline of critical steps of pyrimidine biosynthesis **(I)** Heat map demonstrating differential expression of metabolites in pyrimidine biosynthetic pathway between CFs treated with vehicle MCndM or ENPP1+ATP MCndM (n=3). **(J)** Rescue of cell death following addition of orotidine monophosphate (OMP) to CFs treated with ENPP1+ATP MCndM (filled and unfilled arrows) and **(K)** quantitation of cell death (n=4). Scale Bar: 50 μm. **(L)** Effect on cell death following addition of DHODH inhibitor brequinar (filled arrows) to disrupt pyrimidine biosynthesis and rescue with uridine (unfilled arrows) **(M)** Flow cytometry to determine effects of brequinar on cell death and rescue by uridine (n=5). Scale Bar: 50 μm. Data are expressed as mean ± S.E.M.**p<0.01, *p<0.05, Statistics was determined using Student's t-test, 2 tailed **(B, I) or** Ordinary one-way ANOVA with Tukey's multiple comparison test **(E, G, K, M).**

Figure 9

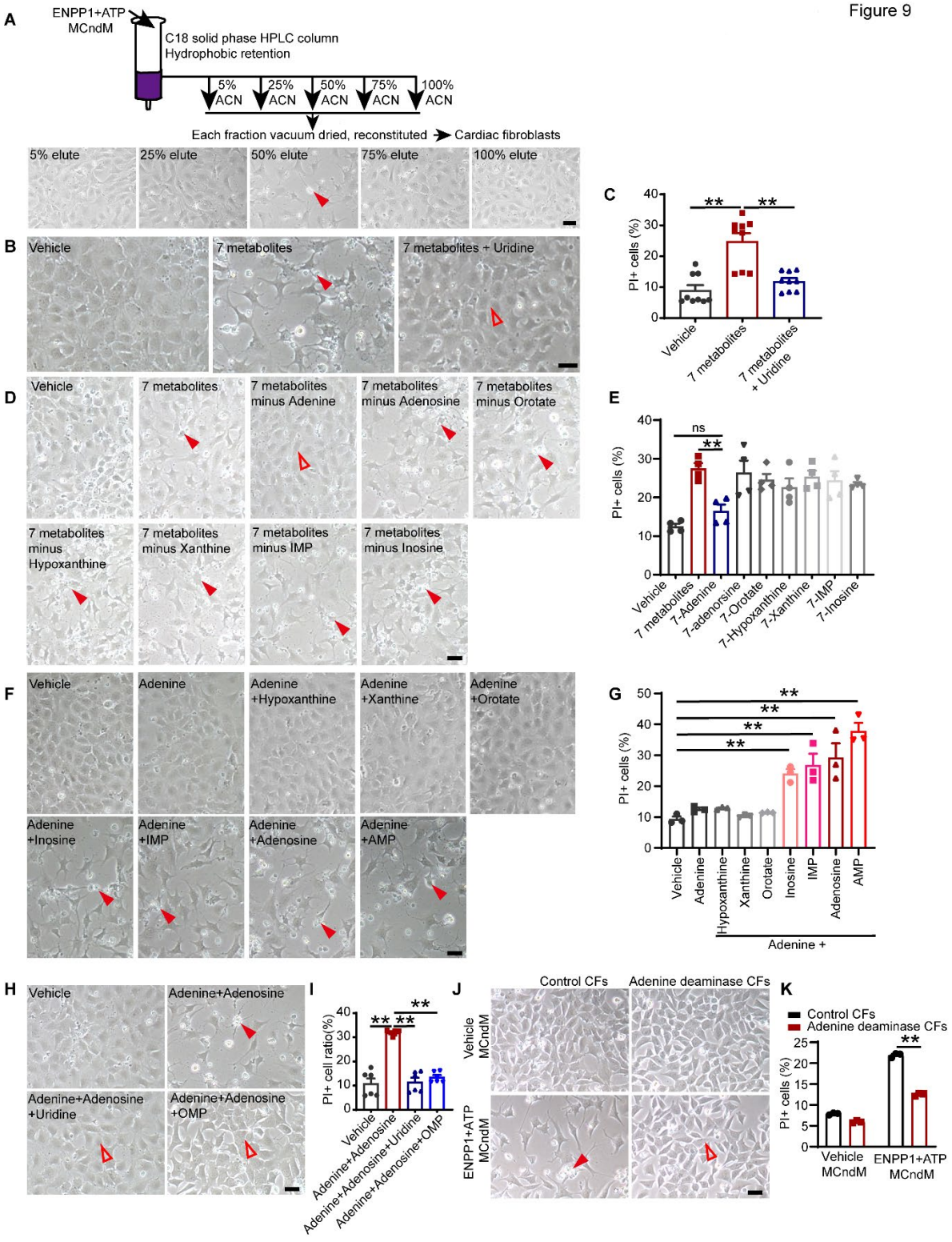
A
ENPP1+ATP
MCndM
C18 solid phase HPLC column
Hydrophobic retention
5% ACN
25% ACN
50% ACN
75% ACN
100% ACN
Each fraction vacuum dried, reconstituted
Cardiac fibroblasts
5% elute
25% elute
50% elute
75% elute
100% elute
B
Vehicle
7 metabolites
7 metabolites + Uridine
C
PI+ cells (%)
Vehicle
7 metabolites
7 metabolites + Uridine
D
Vehicle
7 metabolites
7 metabolites minus Adenine
7 metabolites minus Adenosine
7 metabolites minus Orotate
7 metabolites minus Hypoxanthine
7 metabolites minus Xanthine
7 metabolites minus IMP
7 metabolites minus Inosine
E
PI+ cells (%)
ns
Vehicle
7 metabolites
7-Adenine
7-adenorsine
7-Orotate
7-Hypoxanthine
7-Xanthine
7-IMP
7-Inosine
F
Vehicle
Adenine
Adenine +Hypoxanthine
Adenine +Xanthine
Adenine +Orotate
Adenine +Inosine
Adenine +IMP
Adenine +Adenosine
Adenine +AMP
G
PI+ cells (%)
Vehicle
Adenine
Hypoxanthine
Xanthine
Orotate
Inosine
IMP
Adenosine
AMP
Adenine +
H
Vehicle
Adenine+Adenosine
Adenine+Adenosine +Uridine
Adenine+Adenosine +OMP
I
PI+ cell ratio(%)
Vehicle
Adenine+Adenosine
Adenine+Adenosine+Uridine
Adenine+Adenosine+OMP
J
Control CFs
Adenine deaminase CFs
Vehicle MCndM
ENPP1+ATP MCndM
K
Control CFs
Adenine deaminase CFs
PI+ cells (%)
Vehicle MCndM
ENPP1+ATP MCndM

Figure 9. Adenine and specific purine ribonucleosides are myocyte derived pro-apoptotic molecules that in combination cause cell death of non-myocytes. (A) Effects of eluted fractions of ENPP1+ATM MCndM on cell death (arrows) of CFs. Scale Bar: 50 μm. **(B)** Effect of 7 metabolites on cell death (filled arrows) of CFs and its rescue (unfilled arrows) by uridine and **(C)** quantitation of cell death (n=9). Scale Bar: 50 μm. **(D)** Effects on cell death (filled arrows) of CFs treated with 7 compounds together and following subtraction of each one from the combined solution demonstrates absence of cell death when adenine (unfilled arrow) is removed Scale Bar: 50 μm. **(E)** quantitation of cell death (n=4). **(F)** Effects of cell death (filled arrows) following addition of adenine alone or adenine combined with specific purine nucleosides or orotate and **(G)** quantitation of cell death (n=3). Scale Bar: 50 μm. **(H)** Effect of OMP or uridine in rescuing cell death following addition of adenine and adenosine to CFs (filled and unfilled arrows) and **(I)** Quantitation of cell death (n=6). Scale Bar: 50 μm. **(J)** CFs over-expressing yeast adenine deaminase treated with vehicle MCndM or ENPP1+ATP MCndM showing decreased cell death of CF overexpressing adenine deaminase (filled and unfilled arrows) **(K)** Quantitation of cell death (n=3). Scale Bar: 50 μm. Data are expressed as mean ± S.E.M. **p<0.01, *p<0.05, ns: not significant, Statistics was determined using Student's t-test, 2 tailed **(K) or** Ordinary one-way ANOVA with Tukey's multiple comparison test **(C, E, G, I).**

Figure 10

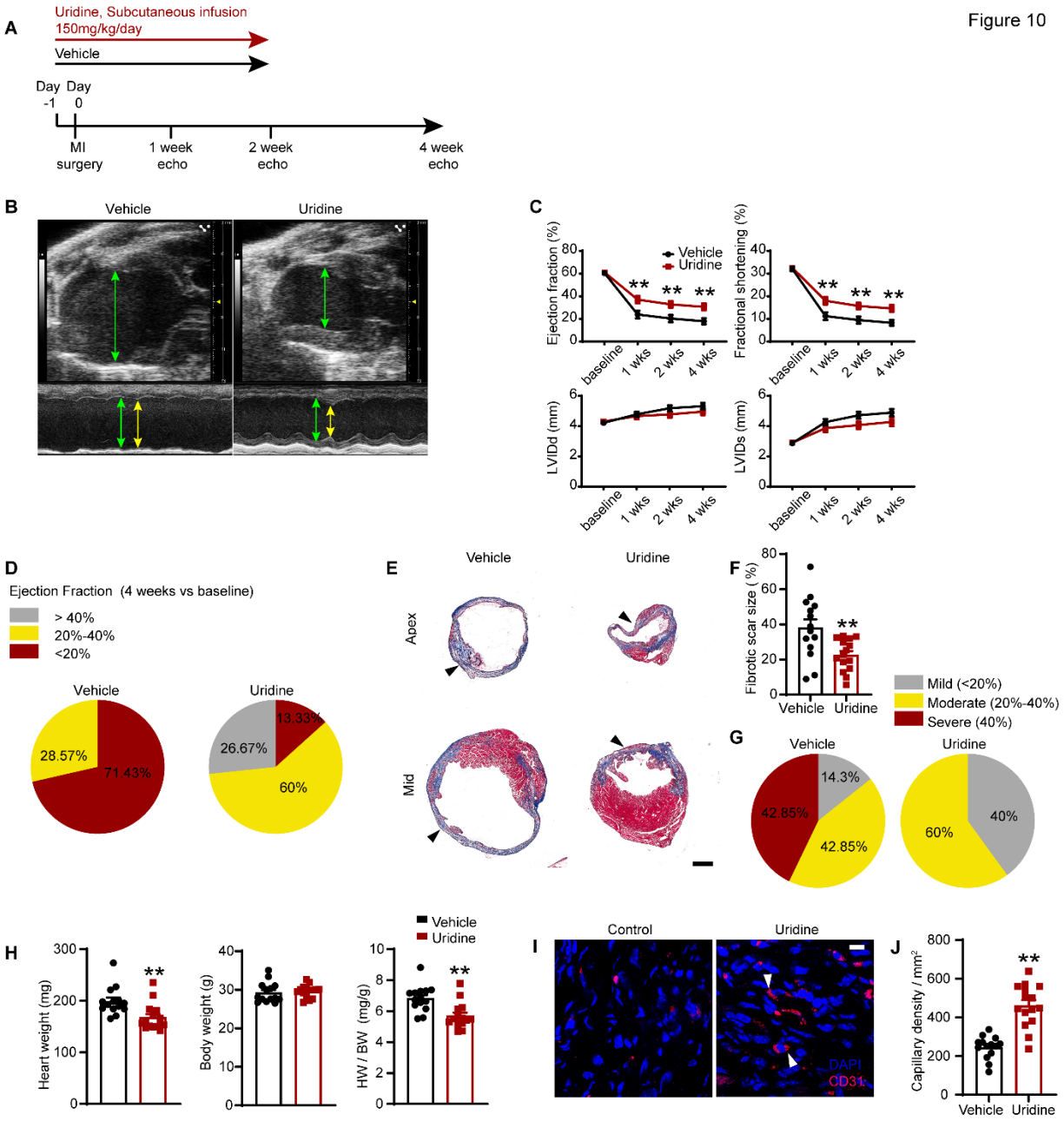
A
Uridine, Subcutaneous infusion
150mg/kg/day
Vehicle
Day -1
Day 0
MI surgery
1 week echo
2 week echo
4 week echo
B
Vehicle
Uridine
C
Ejection fraction (%)
Fractional shortening (%)
LVIDd (mm)
LVIDs (mm)
Vehicle
Uridine
baseline
1 wks
2 wks
4 wks
D
Ejection Fraction (4 weeks vs baseline)
> 40%
20%-40%
<20%
Vehicle
Uridine
28.57%
71.43%
26.67%
13.33%
60%
E
Vehicle
Uridine
Apex
Mid
F
Fibrotic scar size (%)
Vehicle
Uridine
Mild (<20%)
Moderate (20%-40%)
Severe (40%)
G
Vehicle
Uridine
14.3%
42.85%
42.85%
60%
40%
H
Heart weight (mg)
Body weight (g)
HW / BW (mg/g)
Vehicle
Uridine
I
Control
Uridine
DAPI
CD31
J
Capillary density / mm2
Vehicle
Uridine

Figure 10. Pyrimidine supplementation with systemic uridine administration is associated with significantly better cardiac repair and post injury heart function (A) Schematic of continuous uridine administration by a subcutaneous pump starting one day prior to injury and continuing for 14 days after **(B)** B and M-Mode echocardiogram demonstrating better preservation of contractile function during diastole (green line) and systole (yellow line) in uridine injected animals **(C)** Ejection fraction and fractional shortening and left ventricular internal diameter in systole (s) and diastole (d) following uridine administration (n=15/vehicle and 15/uridine at basal, 1 week, 2 weeks and 3 weeks, n=14/vehicle and 15/uridine at 4 week). **(D)** Pie chart demonstrating fraction of animals with mild, moderate and severe reductions in EF following vehicle or uridine administration. **(E)** Masson trichrome staining demonstrating scar size (blue) at apex and mid ventricles of vehicle or uridine injected animals and **(F)** quantitation of differences in scar size as a fraction of the left ventricular surface area (n=14/vehicle and 15/uridine). **(G)** Pie chart demonstrating fraction of animals demonstrating mild, moderate and severe fibrosis following vehicle or uridine administration **(H)** Heart weight, body weight and HW/BW ratio in vehicle versus uridine treated animals (n=14/vehicle and 15/uridine). **(I)** Histology demonstrating capillaries (CD31 staining) in injured regions of hearts 4 weeks after injury in vehicle or uridine treated animals and **(J)** quantitation of capillaries (n=14/vehicle and 15/uridine). Scale Bar: 10 μm. Data are expressed as mean ± S.E.M. **p<0.01, Statistics was determined using Ordinary two-way ANOVA with Šídák's multiple comparisons test **(C)** or Student’s t-test, 2 tailed **(F, H, J).**

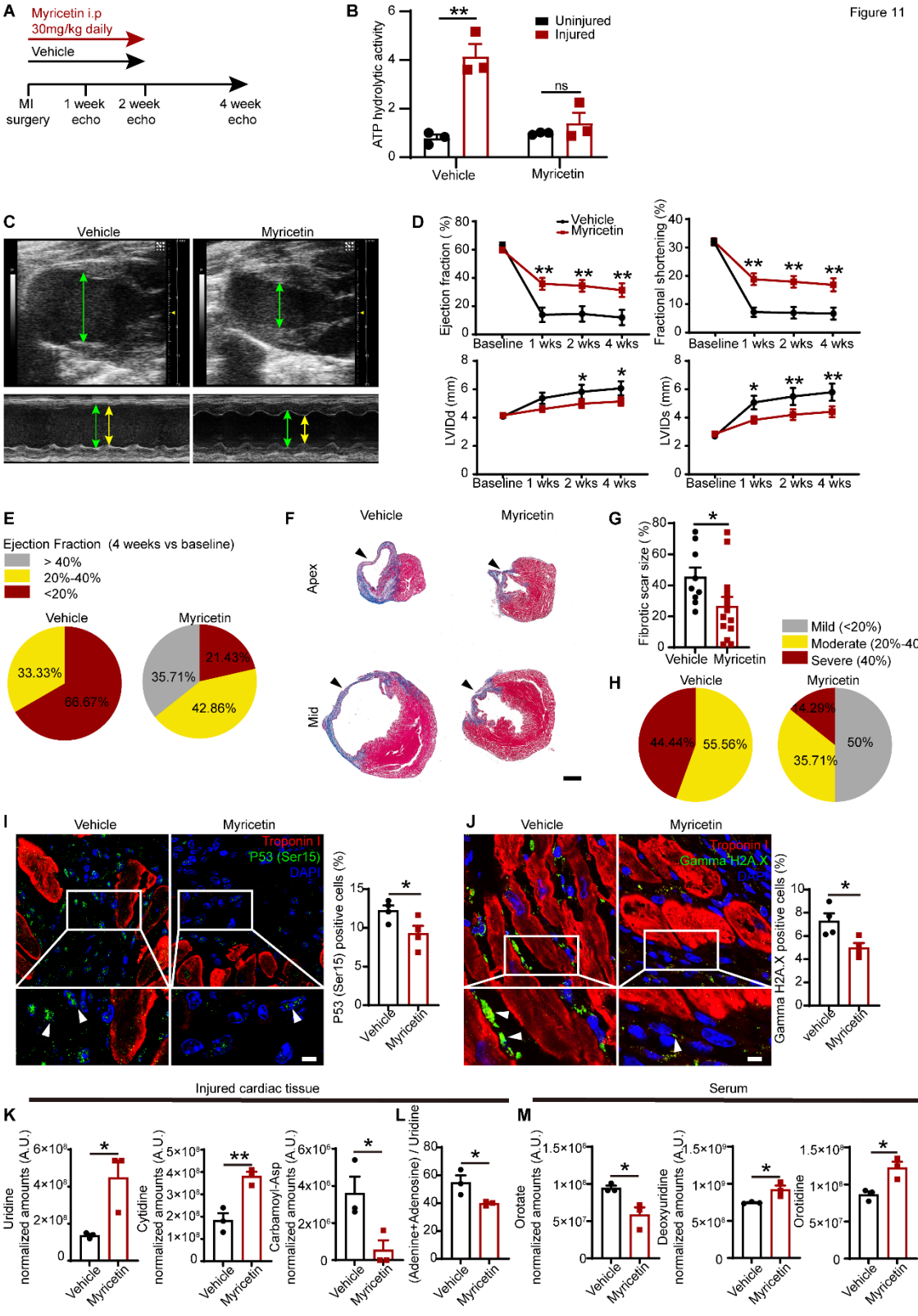
A
Myricetin i.p
30mg/kg daily
Vehicle
MI surgery
1 week echo
2 week echo
4 week echo
B
ATP hydrolytic activity
Uninjured
Injured
**
ns
Vehicle
Myricetin
C
Vehicle
Myricetin
D
Vehicle
Myricetin
Ejection fraction (%)
Fractional shortening (%)
LVIDd (mm)
LVIDs (mm)
Baseline 1 wks 2 wks 4 wks
E
Ejection Fraction (4 weeks vs baseline)
> 40%
20%-40%
<20%
Vehicle
Myricetin
33.33%
66.67%
35.71%
21.43%
42.86%
F
Vehicle
Myricetin
Apex
Mid
G
Fibrotic scar size (%)
Vehicle Myricetin
Mild (<20%)
Moderate (20%-40%)
Severe (40%)
H
Vehicle
Myricetin
44.44%
55.56%
14.29%
50%
35.71%
I
Vehicle
Myricetin
Troponin I
P53 (Ser15)
DAPI
P53 (Ser15) positive cells (%)
J
Vehicle
Myricetin
Troponin I
Gamma H2A.X
DAPI
Gamma H2A.X positive cells (%)
Injured cardiac tissue
Serum
K
Uridine normalized amounts (A.U.)
Cytidine normalized amounts (A.U.)
Carbamoyl-Asp normalized amounts (A.U.)
L
(Adenine+Adenosine) / Uridine
M
Orotate normalized amounts (A.U.)
Deoxyuridine normalized amounts (A.U.)
Orotidine
Vehicle
Myricetin

Figure 11

Figure 11. Animals treated with ENPP1 inhibitor myricetin demonstrate significant improvement in heart function after injury. (A) Strategy for using myricetin **(B)** Extracellular ATP hydrolytic activity in injured and uninjured hearts of animals treated with myricetin (n=3). **(C)** B and M-mode echocardiogram demonstrating contractile function in diastole (green line) and systole (yellow line) in hearts of myricetin treated animals **(D)** Ejection fraction, fractional shortening and LV chamber size in systole (s) and diastole (d) in vehicle or myricetin treated animals (n=12/vehicle and 15/myricetin at basal, 1 week and 2 weeks, n=9/vehicle and 14/myricetin at 3 weeks and 4 week). **(E)** Fraction of animals with mild, moderate and severe reduction in EF at 4 weeks after injury **(F)** Scar size as a fraction of LV surface area **(G)** quantitation of scar surface area (n=9/vehicle and 14/myricetin) and **(H)** Fraction of animals with mild, moderate and severe fibrosis following myricetin administration **(I,J)** Immunostaining demonstrating (**I**) p53(Ser15 phosphorylation) expression (arrows) in non-myocytes in the injured region of vehicle vs myricetin injected animals and under higher magnification (myocytes are stained by troponin) and quantification (n=4) **(J)** pH2AX staining in non-myocyte cells (arrows) in vehicle or myricetin injected animals at 7 days following injury, under higher magnification and quantitation (n=4, counts normalized to number of non-myocyte nuclei for I,J) Scale Bar: 5 μm. **(K)** Metabolomic analysis of the hearts of myricetin injected animals **(L)** decreased adenine+adenosine/uridine ratios in myricetin injected animals (n=3). **(M)** Metabolomic analysis of serum demonstrating decreased orotate and increased deoxyuridine (day 3) and increased orotidine (day 7) in myricetin injected versus vehicle injected animals (n=3). Data are expressed as mean ± S.E.M. **p<0.01, *p<0.05, ns: not significant, Statistics was determined using Ordinary two-way ANOVA with Šídák's multiple comparisons test **(D)** or Student’s t-test, 2 tailed **(B, G, I, J, K, L, M).**

Table 1. Nucleosides/bases that were enriched in the 50% ACN elutes of ENPP1+ATP MCndM versus vehicle MCndM.

Nucleotides in 50% ACN eluate	Fold change (ENPP1+ATP MCndM / Vehicle MCndM)
Adenine	1528.64
Adenosine	1277.43
Hypoxanthine	140.33
Xanthine	28.86
Inosine	228.37
IMP	Abundant / not detected
Orotate	Abundant / not detected